Evaluation of different methods of estimating ET for the performance assessment of irrigation schemes

Ramiro Salgado[1*] and Luciano Mateos[2]

[1]Instituto Nacional de Tecnología Agropecuaria-Estación Experimental Agropecuaria Santiago del Estero, Jujuy 850, 4200 Santiago del Estero, Argentina.

[2]Instituto de Agricultura Sostenible, CSIC, Alameda del Obispo, 14080 Córdoba, Spain.

[*]Corresponding author. Email address: salgado.ramiro@inta.gob.ar

ABSTRACT

In the assessment of irrigation schemes, the accuracy of performance indicators related to the water balance could be improved by estimating crop evapotranspiration (ET_c) using remote sensing techniques. The two main remote sensing approaches to estimating ET_c are the surface energy balance and the FAO56-based approach, that uses the ability of vegetation indices (VI) to trace the crop coefficient. Both approaches were evaluated comparatively at the Río Dulce irrigation scheme in Argentina (where the predominant crops are cotton, alfalfa, and maize) using products from the Landsat 7 and 8 sensors provided by the EEFlux application. The first analysis used field-specific, VI-derived basal crop coefficients obtained for 1743 fields using series of 9 to 29 satellite images along the 2014-15 irrigation campaign. The second analysis used 30 fields (grown with cotton and maize) where the actual irrigation schedules in the 2014-15 irrigation campaign were known. A root zone soil water balance was computed in these fields using the FAO56 dual approach with field-specific, VI-derived basal crop coefficients. The ET_c obtained from the water balance was compared with the ET_c estimated using a single crop coefficient approach that uses field-specific VI and takes into account soil evaporation (herein called synthetic approach), and with the ET_c obtained with the METRIC surface energy balance model as facilitated by the EEFlux application. The third analysis was a simulation analysis of errors in the estimation of the ET_c due to the interpolation to daily values of single crop coefficients and basal crop coefficients determined at hypothetical satellite overpass

intervals of longer than one day. The VI-derived basal crop coefficient curves obtained for the 1743 fields of the first analysis were below the locally adopted standard (not field-specific) basal crop coefficient. Crop evapotranspiration in the 8005 ha covered by this analysis was about 20 % higher when applying standard non-field specific curves than when applying VI-derived curves. This difference pointed to the importance of using field-specific estimations of ET_c. In the analysis carried out on the 30 selected fields, the ET_c estimated using the VI-based approach agreed well with the ET_c obtained from the water balance except under water deficit conditions. The crop coefficients obtained for these fields using the METRIC model correlated with those obtained by applying the VI-based method, although the former tended to be higher than the latter in the lower value range. The analysis of interpolation errors showed that when satellite overpass frequency is greater than one week and water deficit is mild or inexistent, the interpolation of crop coefficients (for instance, of those derived from an energy balance) gives errors of ET_c estimations that are greater than those resulting from the VI-based approach. Under water deficit conditions, the VI-based approach systematically overestimates evapotranspiration.

1. Introduction

Irrigation scheme performance assessment is imperative in a world with an increasing population and food demand, where water scarcity is constraining agricultural production more and more, and emerging sectors compete for the available water resources. Several efforts have been made in the last decades to formulate a framework and guidelines for irrigation scheme performance assessment. Relevant examples of these efforts are the Performance Assessment Program of the International Water Management Institute (Molden et al., 1998); the Guidelines for Benchmarking in the Irrigation and Drainage Sector of the International Programme for Technology and Research in Irrigation and Drainage (Malano and Burton, 2001); and the Task Force on Benchmarking of Irrigation and Drainage Projects of the International Commission on Irrigation and Drainage (Malano et al., 2004). A prominent set of performance indicators, the outcome of these efforts, refers to the water balance. These indicators have been widely applied to the internal assessment (e.g., Morábito et al., 1998; Lozano and Mateos, 2008) and benchmarking (e.g., Rodríguez-Diaz et al., 2008; Borgia et al., 2013; Zema et al., 2018) of irrigation schemes. The accuracy of performance indicators related to the water balance could be improved by estimating evapotranspiration (ET) using remote sensing techniques (Bos et al., 2005). Some of the latter's early applications in the evaluation of irrigation scheme performance were carried out in South America (Menenti et al., 1989; Roerink et al., 1997; Bastiaanssen et al., 2001). With the advent of the Google Earth Engine (a computing platform based primarily on satellite imagery that allows users to run planetary-scale geospatial analysis on Google's infrastructure), this type of application is increasingly within the reach of researchers, developers and water managers.

Two main approaches to estimating crop evapotranspiration (ET_c) assisted by remote sensing techniques have become common in agricultural water use studies (González-Dugo et al., 2009; Taghvaeian and Neale, 2011). The first approach partitions the available energy by using the radiometric surface temperature (derived from thermal band imagery) to estimate the sensible heat flux and compute latent heat as a residual to the surface energy balance (e.g., Kustas and Norman, 1996; Bastiaanssen et al., 1998; Allen et al., 2007a). The second approach is based on the ability of multispectral vegetation indices (VI), derived from surface reflectance data, to trace the crop's growth and estimate the crop coefficient (Bausch and Neale, 1989; Pôças et al., 2020). This approach is unable to detect the reduction in ET_c due to stomata closure, but it generates spatially-distributed crop coefficients that, multiplied by a reference evapotranspiration (estimated daily from local weather station data), provide estimates of field-specific potential (stomatal conductance not limited by water deficit) evapotranspiration (González-Dugo et al., 2009).

Various forms of the remote sensing surface energy balance approach have been applied to upscale the estimations of ET to project scale. For example, Droogers and Bastiaanssen (2002) combined the hydrological model SWAP with ET estimated with the SEBAL (Surface Energy Balance Algorithm for Land; Bastiaanssen et al. 1998) model to evaluate the performance of an irrigation district in Turkey. Similarly, Taghvaeian et al. (2018) calculated a water balance, with ET also estimated with SEBAL, to obtain irrigation performance indicators for an irrigation district in Southern California. Allen et al. (2007a) mapped ET across irrigation districts in Idaho, California, and New Mexico using METRIC (Mapping Evapotranspiration at high Resolution with Internalized Calibration; Allen et al., 2007b), and Santos et al. (2008) used the same model for similar purposes in southern Spain. The ReSET (Remote Sensing of Evapotranspiration; Elhaddad and García, 2011) model has been used to map ET across an irrigation district in California (Elhaddad and García, 2014) and to feed a water balance for obtaining irrigation performance assessment indicators in an irrigation district in Spain (Chalghaf et al., 2015). However, the VI-based crop coefficient approach has been used less on a large scale (examples are in González-Dugo et al., 2013 and Segovia-Cardozo et al., 2019) but more for irrigation advisory services (D'Urso et al., 2010; Melton et al., 2012; Calera et al., 2017).

In both approaches, remote measurements are taken at time intervals, which depend on the sensor overpass frequency. To estimate ET_c for dates between measurements, daily interpolation is needed, and the error due to this interpolation may depend on the remote sensing approach used to estimate ET_c. Satellite overpass frequency varies from satellite to satellite. In addition, a compromise between temporal and spatial resolution is needed to meet the goals of agricultural applications. High spatial resolution (< 100 m) is required in most cases for these applications. The number of sensors on board of satellites that meet the condition of high spatial resolution is limited. This limitation is even greater if the energy balance approach is to be used, i.e., if measurements of radiometric surface temperature are needed. A time resolution of less than one week is rare; two to four weeks is common, although the use of constellations of satellites may help in some situations to increase the time resolution. These constraints condition the accuracy of the two main remote sensing approaches to estimating ET_c, making the selection of the method a challenge.

The objective of this study was a comparative evaluation of the two remote sensing approaches for the estimation of ET_c in the performance assessment of irrigation schemes. The two methods evaluated were the FAO56 method (Allen et al., 1998) with crop coefficients derived from a vegetation index (following Mateos et al., 2013), and the METRIC model (Allen et al., 2007a) as executed by the Earth Engine Evapotranspiration Flux (EEFlux) application (Allen et al., 2015). The evaluation used the Río Dulce irrigation scheme (in the province of Santiago del Estero, Argentina) as a study case. First, the study compared estimations of ET_c (for individual crops and for the entire cultivated area of 8005 ha) using standard (not field-specific) crop coefficients with estimations using field-specific, VI-based crop coefficients. Second, in a set of 30 fields where the irrigation schedule was known, the study compared the field-specific, VI-based approach with METRIC. Finally, the study included an evaluation of errors in the estimation of the crop's evapotranspiration due to the interpolation to daily values of single crop coefficients and basal crop coefficients determined at hypothetical satellite overpass intervals of longer than one day. The evaluation of interpolation errors was related to the comparative evaluation of the two remote sensing approaches for ET_c estimation as both approaches were based on measurements made at discontinuous satellite overpass dates, so interpolation at intermediate dates was necessary.

2. Material and Methods

2.1. Remote sensing-based evapotranspiration models

2.1.1. The FAO56 method to obtain K_c and VI-derived K_c

The method proposed by the FAO to estimate ET_c consists of multiplying a reference evapotranspiration by a crop coefficient (Doorenbos and Pruitt, 1977; Allen et al., 1998). Reference evapotranspiration (ET_o) is calculated with the Penman-Monteith equation (Allen et al., 1998) from meteorological variables measured at ground weather stations. The crop coefficient, K_c, is the quotient between the ET_c of the crop concerned and ET_o. Therefore:

$$ET_c = K_c ET_o \quad (1)$$

K_c may be a single coefficient or be split into two components (dual approach), direct evaporation from the soil surface and plant transpiration (Allen et al., 1998):

$$K_c = K_{cb} K_s + K_e \quad (2)$$

where K_{cb} is the basal crop coefficient (addressing plant transpiration under unstressed conditions), K_s quantifies the reduction in crop transpiration due to soil water deficit, and K_e is the soil evaporation coefficient.

The standard procedure (Allen et al., 1998) for developing the K_c and K_{cb} curves requires three-characteristic value: those during the initial stage ($K_{c\ ini}$, $K_{cb\ ini}$), the mid-season stage ($K_{c\ mid}$, $K_{cb\ mid}$) and at the end of the late season stage ($K_{c\ end}$, $K_{cb\ end}$). The curves are constructed by connecting straight-line segments through each of the four growth stages (initial, crop development, mid-season, and late season). Horizontal lines are drawn through $K_{c\ ini}$ in the initial stage and through $K_{c\ mid}$ in the mid-season stage. Straight lines are drawn from $K_{c\ ini}$ to $K_{c\ mid}$ in the course of the crop development stage and from $K_{c\ mid}$ to $K_{c\ end}$ in the course of the late season stage. Herein, the K_c and K_{cb} curves developed like this will be called $K_{c,standard}$ and $K_{cb,standard}$, respectively.

Since both K_{cb} and multispectral VIs obtained by remote sensing techniques represent crop development (Choudhury et al. 1994), K_{cb} can be derived from VI (Bausch and Neale, 1987; Neale et al., 1989). The relation between some VIs and the ground cover fraction (f_c) is approximately linear in the range from bare soil to near full ground cover (Huete et al., 1985; González-Dugo and Mateos, 2008), thus:

$$f_c = \frac{VI - VI_{min}}{VI_{max} - VI_{min}} \quad (3)$$

where VI_{min} and VI_{max} are the values of VI for $f_c = 0$ and $f_c = 1$, respectively. On the other hand, researches have obtained different linear relationships between VIs and K_{cb} (Pôças et al., 2020). Mateos et al. (2013) validated the following normalized form of these linear relationships to obtain the generic expression:

$$K_{cb,VI} = \min\left[K_{cb,max}, \frac{K_{cb,max}}{f_{c,Kcbmax}}\left(\frac{VI - VI_{min}}{VI_{max} - VI_{min}}\right)\right] \qquad (4)$$

According to this equation, the linear increase of K_{cb} with VI is from the value of VI (VI_{min}) corresponding to bare soil ($f_c = 0$) to the value of VI (VI_{max}) corresponding to pure vegetation ($f_c = 1$). $K_{cb,max}$ is the maximum value of K_{cb}, generally equal to $K_{cb,mid}$. $K_{cb,mid}$ corresponds to $f_c = f_{c,max}$ (Pereira et al., 2020ab). If for some reason the crop in the region of interest is different from the standard crop, then a local value of $K_{cb,max}$ can be used in Eq. 10, in this case associated to its specific f_c ($f_{c,Kcbmax}$). Since $f_c = 1$ is not always achieved (Allen and Pereira, 2009), Eq. 4 ensures that the computed K_{cb} does not exceeds $K_{cb,max}$, (achieved at $f_c = f_{c,Kcbmax}$), and also ensures coherence with the FAO-56 method to determine actual K_{cb}. Although Allen et al. (1998) recommended a minimum value of K_{cb} close to 0.15, for simplicity, Eq. 4 assumes $K_{cb} = 0$ for $f_c = 0$. Setting K_{cb} to zero acknowledges the fact that evaporation of bare soil will reduce to zero or nearly zero over extended drying periods (Allen et al., 2005). Anyway, choosing a minimum K_{cb} closer to 0.15 would have required adapting Eq. 4, but the effect on the comparisons presented in this paper would have been negligible.

K_s equals one for unstressed crops. Thus, the potential crop coefficient of a specific crop may be obtained from Eq. 2, making $K_s = 1$. For water-stressed crops, K_s may be computed as (Allen et al., 1998):

$$K_s = \frac{TAW - D_r}{(1 - p)\ TAW} \qquad \text{If } D_r < (1\text{-}p)\ TAW \qquad (5a)$$

$$K_s = 1 \qquad \text{If } D_r \geq (1\text{-}p)\ TAW \qquad (5b)$$

where D_r is the root zone water depletion (mm), TWA is the root zone total available water (mm) and p is the fraction of the TAW below which transpiration is reduced. The depth of the root zone (Z_r, m) may be calculated as:

$$Z_r = Z_{r\ min} + (Z_{r\ max} - Z_{r\ min})\frac{K_{cb}}{K_{cb,max}} \qquad (6)$$

where $Z_{r\,max}$ (m) and $Z_{r\,min}$ (m) are the maximum effective root depth and the effective root depth during the initial stage of crop growth. Therefore, TAW is

$$TAW = 1000(\theta_{FC} - \theta_{WP})Z_r \tag{7}$$

where θ_{FC} and θ_{WP} are the water content at field capacity and wilting point, respectively (in $m^3\ m^{-3}$).

$D_{r,i}$ in Eq. 5a may be computed with a daily water balance in the soil root zone as:

$$D_{r,\,i} = D_{r,\,i-1} + ET_{c,\,i} - P_i - I_i + (RO_i + DP_i) \tag{8}$$

where $D_{r,i}$ is the root zone water depletion at the end of day i (mm), $D_{r,i-1}$ (mm) is the root zone water depletion at the end of the previous day, i-1, and $ET_{c,i}$, P_i, I_i, RO_i, and DP_i are crop evapotranspiration, precipitation, irrigation, rainfall runoff from the soil surface, and water loss out of the root zone by deep percolation, respectively, on day i and expressed in mm. P_i was measured, $ET_{c,i}$ was computed with equations 1 to 5, RO_i was computed with the curve number method (NRCS, 2004), DP_i was estimated as the soil water in excess of field capacity, and I_i was simulated (according to a given irrigation strategy) or measured, depending on the application (sections 2.4 and 2.5).

The soil evaporation coefficient, K_e, is calculated taking into consideration topsoil wetting events (due to irrigation or rainfall) and the availability of energy at the soil surface (Allen et al., 1998):

$$K_e = \min[K_{c\,max} f_{ew}; K_r(K_{c\,max} - K_{cb})] \tag{9}$$

where K_r is an evaporation-reduction coefficient dependent on the cumulative depth of water depleted from the topsoil, $K_{c\,max}$ is the maximum value of K_c, following rain or irrigation (with $K_{cb} = K_{cb\,max}$), and f_{ew} is the fraction of the soil that is both exposed $(1 - f_c)$ and wetted. Following rain or irrigation, $K_r = 1$. As the soil surface dries, K_r is reduced linearly with cumulative evaporation, to become zero when no water is left for evaporation in the upper soil layer (Allen et al., 1998).

Therefore, the application of the dual crop coefficient requires computing a water balance at the upper soil layer and a soil root zone water balance if crop water stress is to be considered. Computing any of the two water balances implies knowing the dates and depths of irrigation and rainfall events on every field, which is rarely viable when dealing with large irrigation areas. In this case, the single crop coefficient approach is more practical since it assumes typical (not field-specific) wetting conditions. However, satellites provide VIs across large irrigation areas at high spatial resolution, thus one may want to profit from field-specific VIs to improve the accuracy and spatial resolution of the estimation of ET_c. The most straightforward alternative would be applying Eq. 1 with K_c estimated using one relationships between VI and K_c. For instance, this was the method chosen by Segovia-Cardozo et al. (2019) to estimate ET_c in Spanish irrigation schemes based on the linear VI-K_c relationship proposed by Calera et al. (2005). Another alternative would be Eq. 2 with K_{cb} obtained from one of the published VI-K_{cb} linear relationships (Calera et al. 2017) and running a water balance to obtain K_e and K_s. This second option, chosen for instance by Pôças et al. (2015), requires knowing or assuming the irrigation schedules of the fields in the area of study. A third option, somehow intermediate between the two previous ones, uses field specific VIs to obtain field-specific $K_{cb,VI}$ (Eq. 4) and then uses approximate soil-wetting information (rainfall data measures at local weather stations and typical irrigation frequencies) to approximate K_c to field-specific conditions. One way to make such an approximation is in Mateos et al. (2013), where the approximate K_c was called the synthetic crop coefficient ($K_{c,synthetic}$) so as not to be confused with the FAO-56 single crop coefficient:

$$K_{c,synthetic} = K_{c,bare\ soil} + (1 - K_{c,bare\ soil})K_{cb,VI} \qquad \text{if } K_{cb,VI} < 1 \tag{10a}$$

$$K_{c,synthetic} = 1 + \frac{K_{c\ max} - 1}{K_{cb,max} - 1}(K_{cb,VI} - 1) \qquad \text{if } K_{cb,VI} \geq 1 \tag{10b}$$

where $K_{c,bare\ soil}$ is K_e computed with Eq. 9 applied to bare soil ($K_{cb} = 0$) and averaged on the time interval corresponding to each satellite overpass for which VI (and thus $K_{cb,VI}$) was available. If $K_{cb,VI} > 1$ on a given date, then $K_{c,synthetic}$ will depend only on the $K_{cb,VI}$ for that date and on the crop-characteristic parameters $K_{c,max}$ and $K_{cb,max}$. Otherwise, $K_{c,synthetic}$ will depend on $K_{cb,VI}$ on the date of concern but also on $K_{c,bare\ soil}$. $K_{c,synthetic}$ will increase with respect to $K_{cb,VI}$ as $K_{c,bare\ soil}$ is lower. The reader may find more details about the rationale behind Eq. 10 in Mateos et al. (2013). Note that crop evapotranspiration estimated using $K_{c,synthetic}$ ($ET_{c,synthetic}$) is field-specific but does not take into account eventual reduction of transpiration due to stomatal closure provoked by water deficit.

2.1.2. Earth Engine Evapotranspiration Flux (EEFlux) application

The Earth Engine Evapotranspiration Flux (EEFlux) application (Allen et al., 2015) uses Landsat imagery archives on the Google Earth Engine platform to calculate the daily evapotranspiration on the 30 × 30 m scale. Automatically calibrated for each Landsat image, EEFlux produces and provides maps of actual ET_c estimations, surface temperature, normalized difference vegetation index (NDVI), reference evapotranspiration, and albedo for any Landsat 5, 7 or 8 scene. Reference evapotranspiration is computed from gridded hourly and daily weather data stored on Earth Engine using the ASCE Standardized Penman-Monteith method (ASCE–EWRI, 2005) (ET_r) and the FAO-56 method (ET_o) (Allen et al., 1998). EEFlux can be freely accessed in https://eeflux-level1.appspot.com/.

The estimation of actual ET_c in EEFlux is based on the METRIC model (Allen et al., 2007a; Irmak et al., 2012). METRIC is a satellite-based image-processing model for calculating actual evapotranspiration based upon the energy balance at the land surface. The latent heat flux (λET) is calculated from the surface energy balance for the moment captured in satellite image acquisition as:

$$\lambda ET = R_n - G - H \tag{11}$$

where G is the soil heat flux, H is the sensible heat flux, and R_n is the net radiation, all units in Wm^{-2}. Net radiation is computed from solar radiation estimation by taking into consideration the atmospheric transmissivity, surface reflectance, and longwave emission balance using satellite shortwave and thermal observation data. Soil heat flux is estimated as a ratio of net radiation using surface conditions such as vegetation and temperature observed by satellite. Sensible heat flux (H, W m^{-2}) is expressed as

$$H = \rho_a c_p \frac{\Delta T}{r_a} \tag{12}$$

where ρ_a (kg m^{-3}) is the air density, c_p (J kg^{-1} K^{-1}) is the specific heat of air at constant pressure, ΔT (K) is the near-surface vertical temperature difference, and r_a (s m^{-1}) is the aerodynamic resistance corresponding to ΔT. METRIC assumes that ΔT can be approximated by a linear relationship of the radiometric surface temperature (T_R, K) (Bastiaanssen et al., 1998):

$$\Delta T = a + b\, T_R \tag{13}$$

where a and b are empirical parameters determined by means of a calibration based on the selection of "hot" and "cold" pixels within the satellite scene (Bastiaanssen et al., 1998). The ΔT values for these two pixels are estimated by rearranging Eq. 12 for the selected "hot" and "cold" pixels and by using Eq. 11 to derive the respective values of H. Following the procedure proposed by Allen et al. (2007a), the "hot" pixel should be bare, dry soil, so λET = 0 and H = Rn - G; and the cold pixel should be a well-watered crop at full cover where λET is assumed to be 5% above that of the alfalfa reference evapotranspiration (ET_r), computed using the standardized ASCE Penman-Monteith equation (ASCE-EWRI, 2005). The resulting evapotranspiration at the moment of the satellite image is used to calculate a fraction of reference evapotranspiration that enables the conversion of the instantaneous value into daily values of actual ET. The latent heat flux is then computed for each pixel at the instant of satellite overpass and is readily converted to instantaneous ET (ET_{inst}):

$$\mathrm{ET_{inst}} = 3600\frac{\lambda \mathrm{ET}}{\lambda} \qquad (14)$$

A fraction ET_rF is computed for the time of the satellite overpass:

$$\mathrm{ET_rF} = \frac{\mathrm{ET_{inst}}}{\mathrm{ET_r}} \qquad (15)$$

Finally, EEFlux calculates daily ET_c ($ET_{c,EEFlux}$) for each pixel by multiplying ET_rF by the daily ET_r computed from gridded weather data, assuming consistency between ET_rF at overpass time and ET_rF for the 24-hour period:

$$\mathrm{ET_{c,EEFlux}} = \mathrm{ET_rF}\ \mathrm{ET_r} \qquad (16)$$

The corresponding K_c ($K_{c,EEFlux}$) is calculated as the ratio between $ET_{c,EEFlux}$ and ET_o provided by the EEFlux platform. Note that $ET_{c,EEFlux}$ is field-specific and does take into account eventual reduction of transpiration due to stomatal closure provoked by water deficit.

2.2. Study area

The evaluation of methods for estimating ET_c for the performance assessment of irrigation scheme was carried out in the Río Dulce irrigation scheme (SRRD, acronym in Spanish), located in the province of Santiago del Estero, Argentina, at latitude 27°47′ S and longitude 64°16′ W. The area irrigated in SRRD is around 80,000 ha extending over the river alluvial plain. The climate is semiarid, mesothermal, with a mean annual rainfall of 600 mm, concentrated in summer (Morello and Adámoli, 1974). Maximum monthly rainfall occurs in January (111 mm) and minimum in July (2 mm). Mean annual ET_o is 1300 mm, with peak values in December (5.6 mm d^{-1}) and minimum in June (1.6 mm d^{-1}). Mean annual maximum temperature is 27.5 °C (33.6 °C in January and 20 °C in June), and mean annual minimum temperature is 12.7 °C (3.7 °C in July and 19.6 °C in January). All climatic data are from the Instituto Nacional de Tecnología Agropecuaria (INTA) weather station (Fig.

1). Soils, of alluvial origin, are deep, of a silty loam texture and a low content in organic matter and nitrogen (Angueira and Zamora, 2007; Galizzi et al., 2015). The Río Dulce water is of good quality. Predominant crops are cotton and alfalfa, followed by maize, soybean, wheat, oat and vegetables (onion, melon and watermelon). Water is distributed through an open channel network according to a fixed-rotation delivery schedule with turns every 25 to 30 days, a turnout flow rate of 300 l s^{-1}, and duration of delivery of 50 min ha^{-1}, giving a gross irrigation depth of 90 mm per irrigation. Surface irrigation is the predominant on-farm irrigation method with application efficiency and distribution uniformity of around 70 % (Angella et al., 2011). SRRD is divided into five administrative areas. This study covered two of these subsystems, APAZ-IV (canal San Martín) and El Alto. APAZ-IV includes 15,000 ha with irrigation rights (out of a total area of 70,000 ha equipped for irrigation) while El Alto covers 4,000 ha of which only 2,100 ha have irrigation rights (Fig. 1). The analysis was carried out in the 2014-15 irrigation season. In that season, the main crops in APAZ-IV were alfalfa (58 % of the area with water rights), cotton (27 %) and maize (4 %), while in El Alto the main crops were cotton (67 %) and alfalfa (12 %). Other crops (soybean, onion, melon, watermelon, and oat) were present in both subsystems but occupying relatively small areas.

2.3. Crop, weather, soils, and satellite image data

An updated geographical information system was provided by the Irrigation Service of SRRD, an entity that depends on the provincial government of Santiago del Estero. The geographical information contained conventional maps like roads, rivers, canals, land use, and detailed data about the irrigable plots: total area and area with permanent water right. Crop information for each field was provided by the respective managers of the APAZ-IV and El Alto subsystems for the 2014-15 irrigation season.

Meteorological data to compute daily ET_o with the Penman-Monteith equation (Allen et al., 1998) and daily rainfall were obtained from the weather station of the National Weather Service (SMN) for El Alto and from the INTA weather station for APAZ-IV (Fig. 1).

Soil information was taken from the soil maps of the APAZ-IV area produced by Angueira and Zamora (2007). The soils in the study area, of alluvial origin, are relatively homogeneous. Two similar soil classes (named El Simbol and La María according to the INTA classification; Etchevehere, 1976) occupy most of the area (75% of the total area and about 90% of the cultivated area). The main characteristics of the respective typical soil profiles are in Table 1. The soils, deeper than 1.5 m, do not present restriction to crop root growth. Texture is silty loam. Soil water holding capacity in the typical soil profiles of the El Simbol and La María soil classes is 179 mm m^{-1} and 176 mm m^{-1}, respectively. Soil water contents at field capacity (θ_{FC}) and wilting point (θ_{WP}) were derived from the soil water retention curves provided in Angueira and Zamora (2007) for the typical soil profiles, using the method by Rawles and Brakensiek (1982). The result was essentially the same for both soil profiles. Thus, given the relatively low resolution of the soil maps and the relative homogeneity of the soils, the values of $\theta_{FC} = 0.270$ and $\theta_{WP} = 0.092$ m^3 m^{-3} were used for the whole APAZ-IV subsystem. Regarding El Alto subsystem, although it falls just outside the area covered by the available soil maps, based on the experience of INTA researchers we assumed that most cultivated soils in this subsystem belonged to either El Simbol or La María class. Therefore, in the soil water balances applied to fields in the El Alto subsystem we used the same θ_{FC} and θ_{WP} values obtained for the APAZ-IV subsystem.

A set of 16 NDVI images from Landsat 7 (Path/Row 229/80, 230/79 and 230/80) and 14 NDVI images from Landsat 8 (Path/Row 229/80 and 230/79) was downloaded from EEFlux (Table 2). The images selected were all cloud free. Path/Rows 230/79 and 230/80 covered the entire SRRD (14 images in total) while Path/Row 229/80 (16 images) covered only part of SRRD. The images were re-projected to the Coordinate Reference System POSGAR 98/Argentina 4 - "European Petroleum Survey Group" (EPSG) 22174. Geographical analysis was performed with the QGIS 3.10 (QGIS Development Team, 2019) application, a free and open-source software that supports viewing, editing, and analysis of geospatial data. The images from the same date were merged and clipped to the area of interest with QGIS. Then, the "zonal statistics" tool of QGIS was used to extract the mean NDVI value for each image and crop field date.

2.4. Analyses applied to cultivated fields in SRRD

The first analysis concerned all cultivated fields in El Alto and APAZ-IV (161 and 1582, respectively). $ET_{c,standard}$ (ET_c obtained from the FAO56 standard procedure, using $K_{c,standard}$, i.e., without using remote sensing data), $ET_{c,synthetic}$ (ET_c obtained using VI-derived $K_{c,synthetic}$), and $ET_{c,VIopt}$ (ET_c obtained using $K_{cb,VI}$ and computing K_s and K_e running the water balance simulating optimal irrigation schedule, that is, triggering irrigation when the soil water content reaches the allowable depletion) were calculated for these fields. Soil water contents at field capacity and wilting point were $\theta_{FC} = 0.270$ and $\theta_{WP} = 0.092$ m^3 m^{-3}. The crop parameters taken to apply the FAO56 method are in Table 3, as well as the number of fields and area for each crop. The growing calendars were set based on the information from farmers and subsystem managers. K_c values were taken from FAO56 and adjusted for the frequency of wetting and climatic conditions following the recommendations of FAO56 (Allen et al., 1998) and based on the local knowledge of the first author. Values of $f_{c,max}$ or $f_{c,Kcbmax}$ were not readily available in the literature, thus we set the conservative values of 0.8 for all crops, within the range compiled in the reviews by Pereira et al. (2020ab). $NDVI_{min}$ was specifically obtained from the Landsat images selecting fields with bare soil, and $NDVI_{max}$ was set to 0.9 for all crops based on González-Dugo and Mateos (2008) and Carpintero et al. (2020).

The second analysis used 30 fields (23 of cotton and 7 of maize) for which the actual irrigation schedule and growing itinerary (from planting to harvesting) were available. In these fields, $ET_{c,VIact}$ (ET_c obtained using $K_{cb,VI}$ and computing K_s and K_e running the water balance using actual irrigation depths) was compared with $ET_{c,synthetic}$, and $ET_{c,EEFlux}$. The selected fields were located in the APAZ-IV subsystem (Fig. 1), with their size ranging between 8 and 60 ha. Their soils belonged to the La María soil class, thus the characteristic water contents used in the water balance were $\theta_{FC} = 0.270$ and $\theta_{WP} = 0.092$ m^3 m^{-3}. Cotton planting dates were between November 1 and December 10, 2014, while all selected maize fields were planted on January 1, 2015. The number of irrigations varied between 1 and 4 in the cotton fields and was 2 in the maize fields. For these fields, in addition to the images of NDVI, two other EEFlux products were downloaded: ET_o and $ET_{c,EEFlux}$ (six Landsat 7 - Path/Row 230/79 and 230/80- and five Landsat 8 - Path/Row 230/79) (Table 2). A buffer along the crop field borders was eliminated to prevent external pixel contamination.

2.5. Simulation analysis of interpolation errors

The third analysis was a simulation analysis to evaluate the errors in the estimation of ET_c due to the interpolation to daily values of: 1) K_{cb} (used to obtain $K_{c,synthetic}$); and 2) K_c, both determined at hypothetical satellite overpass intervals of longer than one day. Although the context of the interpolation analysis was the application of satellite imagery to estimate ET_c by the VI- and energy balance-based methods, the analysis did not need to apply those methods or use satellite imagery; it only needed assumptions about the frequency of satellite overpasses and supposedly known ("truth") values of K_{cb} and K_c at the satellite overpass dates.

The first step for the interpolation analysis was depicting the curve representing the daily K_{cb} of an ideal cotton crop grown in the environment of Santiago del Estero, from

November 1 to April 15, under non-limiting conditions. This particular K_{cb} curve was taken as being the "truth" ("truth" as opposed to "interpolated") for the interpolation analysis and named $K_{cb,truth}$. Second, the values of $K_{cb,truth}$ corresponding to dates at intervals of 1, 5, 10, 15, 20, 25, 30, 35 and 40 days were selected. This selection resulted in 9 series of values of "truth" coefficients, supposedly corresponding to their respective satellite overpass frequencies. The number of assumed satellite overpasses during the period of analysis (October 1 to May 1) varied from 212 to 5 (corresponding to assumed satellite revisit time of 1 day and 40 days, respectively). Third, the values of $K_{cb,truth}$ in each series were linearly interpolated to obtain daily estimations of K_{cb} (named $K_{cb,interpolated}$). Fourth, $K_{c,synthetic}$ was calculated from Eq. 10 replacing $K_{cb,VI}$ by $K_{cb,interpolated}$. The value of $K_{c,bare\ soil}$, also necessary to apply Eq. 10, was K_e (Eq. 9) applied to bare soil considering rainfall events and averaged on the time interval centred on each of the assumed satellite overpasses. In order to account for the effect of weather variability, the simulation period was 30 years (July 1, 1988 to June 30, 2018), using weather data from the INTA weather station (Fig. 1). Other parameters needed in Eqs. 9 and 10 were taken from Table 3. Finally, $K_{c,synthetic}$ was multiplied by daily ET_o to obtain daily $ET_{c,synthetic}$.

For the analysis of errors in the interpolation of K_c, the assumed "truth" daily K_c curve of the ideal cotton crop was generated applying the dual crop coefficient approach (Eq. 2) using $K_{cb,truth}$. Since the dual approach requires knowing the soil wetting dates, rainfall was obtained from the INTA weather station and the irrigation dates for the ideal cotton crop were simulated using the soil water balance. The simulation period and weather data were the same as for the analysis of interpolation of K_{cb} used to obtain $K_{c,synthetic}$ (i.e., July 1, 1988 to June 30, 2018, INTA weather station). Therefore, while the analysis used a unique $K_{cb,truth}$ curve, the $K_{c,truth}$ curve varied from year to year. Moreover, two surface irrigation strategies were simulated, consisting of refilling the soil to field capacity when the crop depleted the readily available water (estimated as 65 % of the root zone soil water holding capacity) or 80 % of the root zone soil water holding capacity, for the full and deficit irrigation strategies, respectively. Then, the values of $K_{c,truth}$ corresponding to dates at intervals of 1, 5, 10, 15, 20, 25, 30, 35 and 40 days were selected and the "truth" coefficients of each series were linearly interpolated to obtain daily estimations of crop coefficient (named $K_{c,interpolated}$). Finally, $K_{c,interpolated}$ was multiplied by daily ET_o to obtain daily $ET_{c,interpolated}$.

The interpolation errors were evaluated by means of the root mean square error (RMSE) of daily ET_c and the relative error (RE) of seasonal ET_c. The former was obtained from the square of the difference between the daily values of ET_c obtained using $K_{c,truth}$ and obtained with the corresponding daily values of $K_{c,synthetic}$ or $K_{c,interpolated}$. RE was computed as the relative difference between seasonal ET_c computed using $K_{c,truth}$ and computed with $K_{c,synthetic}$ or $K_{c,interpolated}$.

The connection of the interpolation analysis with the comparison of methods of estimating ET_c carried out in the study case is as follows. The VI-based approach used satellite data to obtain K_{cb} on the days of satellite overpass. If it was assumed that K_{cb} can be derived from VIs accurately, then the $K_{cb,truth}$ curve could be reproduced with complete accuracy using daily VIs. If the temporal frequency of K_{cb} determination ($K_{cb,VI}$) was less than daily, then daily $K_{cb,VI}$ values would have to be obtained by interpolation, thus making interpolation errors. On the other hand, the energy balance approach determined K_c as the quotient between ET_c and ET_o determined on the days of satellite overpass ($K_{c,EEFlux}$ in our study). If it was assumed that this K_c can be obtained with complete accuracy, then the interpolated $K_{c,EEFlux}$ curve would reproduce $K_{c,truth}$ if satellite overpass was daily; otherwise, daily $K_{c,EEFlux}$ values would have to be obtained by interpolation, thus making interpolation errors that would depend on the satellite overpass frequency.

The hypothesis behind the interpolation analysis is as follows. Since the evolution of VIs along the crop growing cycle follows a rather determined trend, K_{cb} can be interpolated confidently between dates of image acquisition. However, the VI-based approach needs a complementary procedure to account for soil wetting events (to obtain $K_{c,synthetic}$ in the approach adopted in this study) and is unable to detect crop water stress. In contrast, the energy balance approach gives the crop coefficient directly, considering effects of water deficit as well, but the interpolation to daily crop coefficients may be unreliable because both numerator and denominator in the quotient ET_c/ET_o used to determine K_c are highly affected by day-to-day weather variability. Therefore, the objective of the interpolation analysis was to assess the errors of each method as a function of the temporal frequency of the satellite images.

This analysis was intended to specifically address the errors due to interpolation; therefore, it did not take into account the inaccuracy of the methods used to determining $K_{cb,VI}$, $K_{c,synthetic}$ and $K_{c,EEFlux}$.

3. Results

3.1. Comparison of methods of estimating ET_c

Fig. 2a shows the FAO56 standard K_{cb} ($K_{cb,standard}$) curve for cotton, consisting of 4 straight lines. The curve was constructed before determining VI, taking the three K_{cb} characteristic values and the duration of the growth stages from Table 3. During the crop development and mid-season stages, $K_{cb,VI}$ was less than $K_{cb,standard}$ in both the APAZ-IV and El Alto subsystems. This can be seen in the mean and standard deviation of the $K_{cb,VI}$ corresponding to the cotton fields in both El Alto and APAZ-IV at the dates of satellite overpass (Fig. 2a). Similar observations are in Fig. 2c for the alfalfa fields. $K_{cb,standard}$ refers to a pristine crop, thus the deviation of $K_{cb,VI}$ from $K_{cb,standard}$ reflects the cropping performance gap and points to the convenience of the field-specific approach for scheme water consumption assessment. Actually, average cotton yield in SRRD is about 3 Tn ha^{-1}, while attainable yield (yield of the best performing crops) is 5 Tn ha^{-1} (Angella et al., 2016). During the late season stage, the mean $K_{cb,VI}$ of cotton was slightly greater than the $K_{cb,standard}$. The declining slope of the late season $K_{cb,standard}$ implies the recommended practice of forcing defoliation to accelerate boll opening. The milder slope of $K_{cb,VI}$ reflects the indeterminate nature of cotton that often regrows during and after the harvesting period, while weeds may proliferate below the cotton canopy (distorting the $K_{cb,VI}$ estimate).

This discussion on K_{cb} can be transferred in the same terms to K_c with the addition that in K_c soil wetting also intervenes. During the cotton development mid-season stages, $K_{c,synthetic}$ was less than $K_{c,standard}$ in both the APAZ-IV and El Alto subsystems (Fig. 2b). During the initial and early cotton development stages, $K_{c,synthetic}$ on the satellite overpass dates (triangles and squares in Fig. 2b) deviated from $K_{c,standard}$, showing that the former takes into account the occurrence of rainfall and dry periods. In the case of alfalfa (Fig. 2d), the locally assumed $K_{c,standard}$, that is based on the cutting frequency in the different seasons, was greater than $K_{c,synthetic}$, especially in winter and autumn. Note that the field-to-field variability of $K_{c,synthetic}$ could be evaluated not only on the dates of the satellite overpass (indicated in Fig. 2bd by standard deviation bars on the days of the satellite overpass), but also on the interpolated dates (as shown in Fig. 2bd with the area shaded by daily standard deviation bars). For the sake of brevity, we restricted the description of standard vs. VI-based K_{cb} and K_c to cotton and alfalfa, the two main crops in SRRD; however, similar analyses would apply to other crops.

Fig. 2b reinforces the recommendation of using the VI-based field-specific approach in SRRD (as Segovia-Cardozo et al., 2019, also remarked for their study area), and the adequacy of the synthetic crop coefficient approach to approximate the effect on K_c of rainfall events when field irrigation data are not available. Alternatively, one could use the dual crop coefficient with $K_{cb,VI}$ and compute the soil evaporation coefficient (Allen et al., 1998) for an arbitrary irrigation schedule.

The results of applying one or other method on a system scale are in Table 4. Seasonal ET_c in APAZ-IV was greater than in El Alto, mainly due to the cropping pattern (alfalfa occupies 58 % of the area in APAZ-IV and 12 % in El Alto). Subsystem ET_c was much greater (about 20 %) when using $K_{c,standard}$. The difference in system ET_c estimated with $K_{c,synthetic}$ and applying the dual crop coefficient with an optimal irrigation schedule ($ET_{c,VIopt}$) was only 2 % (Table 4).

The same comparison is in Fig. 3 for the 30 selected fields with known irrigation schedules. In the sample of cotton fields, $ET_{c,synthetic}$ correlated very well with ET_c estimated from VI and the actual irrigation schedule ($ET_{c,VIact}$) (Fig. 3); however, in the maize fields $ET_{c,synthetic}$ was greater than $ET_{c,VIact}$. Note that the water balance computed to estimate $ET_{c,VIact}$ takes into account ET_c reduction due to water deficit, while the computation of $ET_{c,synthetic}$ ignores it. Fig. 3 suggests that water deficit was more pronounced in the maize fields than in the cotton fields. For economic reasons, in SRRD it is common practice to apply one irrigation only (the pre-irrigation) to the maize crops, and rely on rainfall for the rest of the growing season, while cotton crops typically receive one or two irrigations in addition to the pre-irrigation. Therefore, considering the crop water deficit could be important when estimating ET over systems such as SRRD; however, the VI-based approach is incapable of detecting the reduction in ET due to stomatal closure unless it is coupled to a water balance fed with field-specific irrigation data.

In theory, the energy balance approach to estimating ET_c may overcome this limitation. This was examined for the selected fields with known irrigation schedules. Fig. 4a represents K_c on the days of satellite overpass provided by EEFlux ($K_{c,EEFlux}$) against $K_{c,VIact}$. Overall, $K_{c,EEFlux}$ was greater than $K_{c,VIact}$, particularly at low K_c. Part of this deviation could be due to small differences between the typical values of θ_{FC} and θ_{WP} used in the water balance and the actual values of each selected field; however, this could not be assessed. Part of the scatter (root mean square error, RMSE = 0.23) could be due to differences in the reference evapotranspiration used by EEFlux and that obtained from the weather stations. Recall that EEFlux uses gridded weather data stored in Earth Engine and the ASCE standardized Penman-Monteith equation (ASCE–EWRI, 2005) while the ET_o from the weather stations is computed using measured data and FAO-56 Penman-Monteith equation (Allen et al., 1998). Nevertheless, the correlation between reference evapotranspiration derived from the two sources was unbiased and relatively good, with RMSE = 0.9 mm (Fig. 5).

However, the field irrigation schedules across the SRRD system are unknown. Therefore, field daily ET_c is estimated more adequately using $K_{c,synthetic}$, which is represented vs. $K_{c,EEFlux}$ in Fig. 4b for the selected fields. This figure highlights deviations as a consequence of applying the $K_{c,synthetic}$ method. The symbols circled with a continuous line correspond to satellite overpass dates soon after pre-irrigation and before crop emergence. $K_{c,EEFlux}$ detected the wet soil that resulted in high evapotranspiration (the upper and lower circle mark data points corresponding to 1 and 4 days after pre-irrigation, respectively, while the middle circle indicates data points corresponding to 3 days after pre-irrigation). Conversely, the smoothing feature of $K_{c,synthetic}$ resulted in $K_{c,synthetic}$ less than that actually expected for that soil surface wetness. The opposite circumstance occurred for the five data points circled with a discontinuous line: on that satellite overpass date, the plants were small or had not emerged, the previous soil-wetting event had occurred 6 days before (thus the soil surface was already dry) and a posterior rainfall event occurred 2 days later. In this case, the smoothing feature of $K_{c,synthetic}$ resulted in higher values than those actually expected for the soil surface wetness on the day of the satellite overpass.

The difficulties of applying the energy balance (for instance, using METRIC) have been overcome by platforms like EEFlux; however, the number of satellites providing thermal data remains a limitation. In our analysis of SRRD over a 12 month period, the number of useful Landsat images varied across the scheme from 9 to 29, with frequency varying from biweekly to monthly.

3.2. Interpolation results

The question is, with this frequency of images, which would be more appropriate: to interpolate K_c directly (for instance, output of the energy balance approach) or interpolate K_{cb} (for instance, output of the VI approach) and use an algorithm to derive K_c (for instance, the synthetic method). Fig. 6 depicts daily K_{cb} and K_c for the ideal cotton crop that represents the "truth" in the interpolation analysis that follows ($K_{cb,truth}$ and $K_{c,truth}$, respectively). The irrigation strategy in Fig. 6 was full irrigation. $K_{cb,interpolated}$ and $K_{c,interpolated}$ resulted from the linear interpolation of their respective "truth" values on the assumed days of satellite overpass (marked by diamonds at the top of each Fig. 6), and $K_{c,synthetic}$ resulted from applying the synthetic methodology using $K_{cb,interpolated}$ as an input. $K_{cb,interpolated}$ and $K_{c,interpolated}$ would coincide with the respective "truth" coefficients if the satellite overpass were to be daily. Fig. 6a presents the five crop coefficient curves assuming an overpass interval of 15 days. The main observations were that $K_{cb,interpolated}$ represented $K_{cb,truth}$ very well; $K_{c,interpolated}$ fluctuated greatly capturing some of the variations of $K_{c,truth}$ but missing others; and $K_{c,synthetic}$ smoothed the fluctuations of $K_{c,truth}$.

Similarly, Fig. 6b presents the same five crop coefficient curves although assuming an overpass interval of 35 days. $K_{cb,interpolated}$ still represented $K_{cb,truth}$ quite well; $K_{c,interpolated}$ deviated highly from $K_{c,truth}$ during most days of the initial and crop development stages; and $K_{c,synthetic}$ smoothed the fluctuations of $K_{c,truth}$ to a curve that was even flatter than that generated for the overpass interval of 15 days. This was just an example resulting from the specific rainfall pattern and irrigation schedule of a specific year. Fig. 7 shows the RMSE of the estimation of daily ET_c with the water balance run for the 30 years of weather data under the full irrigation strategy, using either $K_{c,interpolated}$ or $K_{c,synthetic}$. For short overpass intervals, the RMSE result of using $K_{c,synthetic}$ was greater than that employing $K_{c,interpolated}$. The curves crossed at an overpass interval of about 4 days, reaching a practically constant difference of about 0.3 mm day^{-1} for overpass intervals longer than 10 days. Although the difference between both RMSE was relatively small, it was noticeable that the standard deviation of RMSE was greater using $K_{c,interpolated}$ than using $K_{c,synthetic}$.

RE of seasonal $ET_{c,synthetic}$ was close to zero and showed little year-to-year variability when the water balance was run to prevent water deficit (Fig. 8a); however, under the deficit irrigation strategy, seasonal $ET_{c,synthetic}$ was systematically greater (bias of about 5 %) than the seasonal ET_c obtained from $K_{c,truth}$ (Fig. 8b). Contrarily, the RE of seasonal ET_c obtained from $K_{c,interpolated}$ did not differ from zero and was similar under full irrigation and deficit irrigation; however, year-to-year variability was notably large. This is important because one of the advantages of the energy balance approach is its capacity to detect ET_c reduction due to crop water stress.

Fig. 9a compares seasonal $ET_{c,EEFlux}$ with $ET_{c,VIact}$ computed for the 2014-15 irrigation season on the 30 selected fields. The satellite overpass interval for these computations varied from 24 to 66 days. It can be observed that cotton seasonal $ET_{c,EEFlux}$ was greater overall than the corresponding $ET_{c,VIact}$ (Fig. 9a). The RMSE of seasonal $ET_{c,EEFlux}$ vs. seasonal $ET_{c,VIact}$ was 75 mm and 27 mm for cotton and maize, respectively. The three satellite images that were available during the initial and early cotton development stages coincided in that particular year with dates immediately after rainfall events, so that $K_{c,interpolated}$ during that period was greater than $K_{c,VIact}$ on most days (an example of $K_{c,interpolated}$ representative of this circumstance is in Fig. 10a). The opposite occurred for the maize fields. In the 2014 cropping season, satellite overpasses during the initial and early cotton development stages coincided with dates several days after rainfall events, when the soil surface was already dry, so that the $K_{c,interpolated}$ during that period was lesser than $K_{c,VIact}$ on most days. However, this deviation is not visible in Fig. 9a because the underestimation consequence of the interpolation effect was compensated for by an overestimation of ET_c during the mid-season and late season stages, when the maize crops suffered water deficit but the last satellite overpasses occurred before the deficit period (an example of $K_{c,interpolated}$ representative of the two counteracting circumstances in the maize crops is in Fig. 10b).

Similarly to Fig. 9a, Fig. 9b compares seasonal $ET_{c,EEFlux}$ with $ET_{c,synthetic}$. The smoothing effect of $K_{c,synthetic}$ slightly reduced the discrepancy between the two approaches. This was evident for the cotton crops although the maize data points that in Fig. 9a were close to the 1:1 line, in Fig. 9b were below that line (the RMSE of seasonal $ET_{c,EEFlux}$ vs. seasonal $ET_{c,synthetic}$ was 74 mm and 83 mm for cotton and maize, respectively). This reflects the incapacity of the $K_{c,synthetic}$ method to account for the reduction in ET_c as a consequence of the eventual crop water deficit.

4. Discussion

The standard deviation bars in Figs. 2a and 2c depict an important field-to-field crop growth variation. Other authors have observed it, as well as its implications for crop water use. Using a time series of SPOT and Landsat NDVI images, Simonneaux et al. (2008) and Er-Raki et al. (2010) classified winter wheat into classes that differed greatly within an irrigation scheme in central Morocco. Seasonal evapotranspiration for those wheat classes varied between 200 and 450 mm, a range of the same order as that obtained in our study using similar methodology. For instance, in the APAZ-IV and El Alto subsystems, $ET_{c,synthetic}$ varied between 437 and 902 mm and between 512 and 795 for cotton and maize fields, respectively. Tasumi et al. (2005) and Tasumi and Allen (2007) also reported growth variation in a variety of irrigated crops in Idaho using Landsat NDVI images. These authors did not used NDVI-derived K_c but obtained K_c directly by using an energy balance approach. Field-to-field ET_c variation was not discussed in these studies although the results showed that early-planted crops consumed more water than late-growing ones (Tasumi and Allen, 2007), but in a narrower range than that observed in the APAZ-IV and El Alto subsystems. These findings and similar ones by other authors (e.g., Santos et al., 2008; Gonzalez-Dugo et al., 2013; French et al., 2018; Segovia-Cardozo et al., 2019) stress the importance of exploring factors that influence irrigation decisions (Gibson et al., 2018), and of going deeper into methodologies to accurately determine spatially-distributed water use in irrigation schemes.

A crucial issue when determining ET_c by using methods based on remote sensing is soil evaporation under partial ground cover. Tasumi et al. (2005) observed that the variation in the K_c curves was considerably greater than that for the NDVI, which they attributed to the effect of wetting events on K_c, particularly during the initial and developmental growth stages. Methods based on VI are adequate for deriving K_{cb} but not for the soil evaporation component of K_c. Therefore, some complementary algorithm is necessary to overcome this limitation. One alternative is to run a water balance (Pôças et al., 2015) as we did to compute $ET_{c,VIopt}$ (for the entire subsystems) and $ET_{c,VIact}$ (for selected fields); however, this requires additional soil information and knowing the irrigation dates of each field, which are rarely available on a scheme scale. The synthetic crop coefficient (Mateos et al., 2013) adopted in this study overcame this shortcoming by computing crop coefficients that took into account field specific K_{cb} while adjusting K_c to actual rain wetting events and typical irrigation frequency. The $K_{c,synthetic}$ curve depicted in Figs. 2b and 2d sounds like a realistic temporal evolution, first, better adjusted to local conditions than the $K_{c,standard}$ curve and, second, capturing the field-to-field variation that the $K_{c,standard}$ cannot do. The similarity of seasonal $ET_{c,VIopt}$ and $ET_{c,synthetic}$ in the APAZ-IV and El Alto subsystems (Table 4) and the good correlation between seasonal $ET_{c,VIact}$ and $ET_{c,synthetic}$ for cotton crops (Fig. 3) support the use of the $K_{c,synthetic}$ methodology. Even if only partially, this methodology approximates the single and dual crop coefficients that are so discrepant when ground cover is partial (López-Urrea et al., 2009). Additionally, the potential for better adjusting $K_{c,standard}$ to local conditions using a remote sensing approach (Tasumi et al., 2005; Segovia-Cardozo et al., 2019) was evident in SRRD.

It was notable how the synthetic approach missed the effect of deficit irrigation of maize (Fig. 3). This observation prompted the comparison with an energy balance approach. EEFlux was a helpful and friendly platform allowing non-experts to apply METRIC. The comparison of $K_{c,EEFlux}$ with $K_{c,VIact}$ in Fig. 4a indicated that the former was greater than the latter in the range of smaller values. Ayyad et al. (2019) obtained similar results when comparing EEFlux with other satellite-based models in irrigated areas of Egypt. One of the causes of this discrepancy could be the difference between METRIC and EEFlux. Firstly, EEFlux uses gridded weather data to estimate reference evapotranspiration, while METRIC and the VI-based approach use data from weather stations. Secondly, some authors have observed that the automated EEFlux calibration algorithm could require some adjustment to reproduce manually-calibrated METRIC products for certain environments (Foolad et al., 2018). Nevertheless, the RMSE of 0.22 found in our comparison of $K_{c,EEFlux}$ with $K_{c,synthetic}$ was of the same order as the results of other authors who compared METRIC with other models. For instance, French et al. (2015) found that METRIC ET_c estimates agreed with ET_c obtained from consecutive measurements of soil water content in cotton to about 2 mm d^{-1}. Paço at al. (2014) stated that ET_c of an olive orchard hedgerow computed using the FAO56 method agreed rather well with METRIC ET_c estimations. The deviation of the crop coefficients obtained with METRIC and with the FAO56 model developed by these authors (mean bias of 18 %) was similar or even greater than the deviation observed in our comparison. Zhang et al. (2015) found a good correlation between METRIC ET_c estimates of sugarcane with those of ET_c computed with the FAO56 method using a VI-derived K_{cb} (RMSE = 0.17-0.19 mm d^{-1}), although the former was lesser than the latter in the range of lower ET_c. However, K_c obtained from METRIC agreed quite well with K_c derived from VI in the two sugarcane fields monitored by these authors. Nevertheless, other authors who carried out inter-comparison of models observed greater discrepancies. For instance, Al Zayed et al. (2016) obtained a RMSE of 2 mm d^{-1} when comparing METRIC ET_c with ET_c derived from a water balance in the Gezira irrigation scheme (Sudan), with the former globally greater than the latter. Similarly, French et al. (2018) compared METRIC ET_c with estimates of ET_c computed with the FAO56 method (using VI-derived K_{cb}) obtaining that the former was about 1 and 2 mm d^{-1} greater than the latter for alfalfa and cotton, respectively, implying a significant deviation when computing seasonal ET_c.

However, the main source of error in the estimation of seasonal ET_c may derive from interpolation between spaced dates due to infrequent satellite overpass. He et al. (2017) compared METRIC ET_c estimates over an almond orchard in California with measurements taken with a micrometeorological tower. Satellite revisiting time was 16 days, but most images during December to March were not usable due to cloud cover. The conditions of the orchard were the ones that minimize the interpolation error (adult and uniform orchard, no rainfall, micro-irrigation). However, the mean relative difference of monthly aggregations from April to September was 10 %, within the range estimated in Fig. 8a for 15-day revisiting time. French et al. (2015) tested the impact of overpass frequency on cotton seasonal ET accuracy and showed a significant advantage in an 8-day overpass frequency compared with a 16-day observation interval. Similar results by Zhang et al. (2015) led these authors to conclude that the VI approach may be more practical for estimating sugarcane crop water use, where ground-based ET_o measurements are available through on-site weather stations. Our results support this conclusion except under the following circumstances: when satellite-revisiting time is less than one week; if deficit irrigation is a common practice; or where ground-based ET_o measurements are not available through automated weather stations or in a network covering all the scheme's conditions. The first condition was not met in SRRD but the other two were. The distance from SRRD fields to the nearest weather station may be up to 5 km, and the perception of farmers and agriculturalists is that significant weather variations are evident across the scheme on specific days. Thus, as concluded by Zhang et al. (2015) for a different environment, spatially distributed reference evapotranspiration (in this case provided by EEFlux) seems to be a better choice in SRRD than reference evapotranspiration obtained at the weather stations.

In summary, a combination of the two approaches evaluated in this study could be the best option, as suggested by Paço et al. (2014). Meanwhile, it is clear that scheme performance assessment based on ET_c estimations interpolating satellite-derived K_c is subject to errors that advise against such applications.

5. Conclusions

In the assessment of irrigation schemes, water balance-related performance indicators could be notably improved if the crop evapotranspiration estimated is field-specific, and based on remote sensing techniques. The robustness of the VI-based approach is the confidence of the daily interpolation of the VI-derived K_{cb}. Its disadvantages are the need of a complementary procedure to account for soil wetting events and its inability to detect crop water stress. Therefore, if deficit irrigation is a common practice (as observed in some crops in SRRD), the VI-approach will overestimate crop evapotranspiration so that remote sensing methods based on the energy balance may be more appropriate. However, when satellite overpass frequency is greater than one week (and water deficit is mild or inexistent), the interpolation of crop coefficients obtained with the energy balance approach leads to errors of ET_c estimations that are greater than the errors resulting from estimating ET_c using VI-derived basal crop coefficients in combination with an algorithm to consider soil evaporation. The synthetic crop coefficient was an appropriate approach to deriving field-specific VI-based crop coefficients when the dates of field irrigation events are unknown, as commonly happens in large irrigation schemes, although other VI-based approaches may be as appropriate as the synthetic crop coefficient.

Future research should therefore investigate methods to combine both approaches to take advantage of the robustness of each of them avoiding their weaknesses.

Acknowledgements

The first author acknowledges the grant funded by INTA to develop his PhD at the Instituto de Agricultura Sostenible (CSIC) in Spain.

List of symbols and acronyms

c_p: specific heat of air at constant pressure [J kg^{-1} K^{-1}]

D_r: root zone water depletion [mm]

DP: water loss out of the root zone by deep percolation [mm]

ET: evapotranspiration [mm d^{-1}]

$ET_{c,interpolated}$: crop evapotranspiration obtained using $K_{c,interpolated}$ [mm d^{-1}]

$ET_{c,EEFlux}$: crop evapotranspiration obtained from the EEFlux platform [mm d^{-1}]

$ET_{c,standard}$: crop evapotranspiration obtained from the FAO56 standard procedure, using $K_{c,standard}$ [mm d^{-1}]

$ET_{c,synthetic}$: ET_c obtained using $K_{c,synthetic}$ [mm d^{-1}]

$ET_{c,VIact}$: ET_c obtained using $K_{cb,VI}$ and computing K_s and K_e running a water balance for a given irrigation schedule [mm d^{-1}]

$ET_{c,VIopt}$: ET_c obtained using $K_{cb,VI}$ and computing K_s and K_e running a water balance for an optimal irrigation schedule that simulates irrigation when the soil water content reaches the allowable depletion [mm d^{-1}]

ET_c: crop evapotranspiration [mm d^{-1}]

ET_{inst}: instantaneous evapotranspiration flux at the time of satellite overpass [mm h^{-1}]

ET_o: (grass) reference crop evapotranspiration [mm d^{-1}]

ET_r: alfalfa reference crop evapotranspiration [mm d^{-1}]

ET_rF: reference ET fraction calculated as the ratio of the computed instantaneous ET_{inst} from each pixel to the instantaneous reference ET_r (mm h^{-1}) [-]

$f_{c,max}$: f_c corresponding to $K_{cb\ mid}$ [-]

$f_{c,Kcbmax}$: f_c corresponding to $K_{cb,max}$ [-]

f_c: fraction of soil surface covered by vegetation (as observed from overhead) [-]

f_{ew}: fraction of soil that is both exposed and wetted (from which most evaporation occurs) [-]

G: soil heat flux [W m^{-2}]

H: sensible heat flux [W m^{-2}]

I: Irrigation depth [mm]

$K_{c\ end}$: crop coefficient at end of the late season growth stage [-]

$K_{c\ ini}$: crop coefficient during the initial growth stage [-]

$K_{c\ mid}$: crop coefficient during the mid-season growth stage [-]

$K_{c,VI}$: crop coefficient obtained from VI [-]

$K_{c,VIact}$: crop coefficient obtained from $K_{cb,VI}$ and computing K_s and K_e running a water balance for a given irrigation schedule [-]

$K_{c,bare\ soil}$: crop coefficient for bare soil [-]

$K_{c,EEFlux}$: crop coefficient obtained from dividing $ET_{c,EEFlux}$ by reference evapotranspiration provided by EEFlux [-]

$K_{c,interpolated}$: daily K_c obtained by interpolation of K_c determined on days of satellite overpass [-]

$K_{c,max}$: maximum value of crop coefficient (following rain or irrigation) [-]

$K_{c,standard}$: crop coefficient obtained from segmented crop coefficient curve determined by the values of K_c at the initial, mid-season and end-season, respectively $K_{c\ ini}$, $K_{c\ mid}$ and $K_{c\ end}$ [-]

$K_{c,truth}$: crop coefficient simulated with the daily water balance using the dual approach and assumed to be the "true" value for the interpolation analysis [-]

$K_{c,synthetic}$: crop coefficient obtained from $K_{cb,VI}$ and Eq. 6 [-]

K_c: crop coefficient [-]

$K_{cb\ end}$: basal crop coefficient at end of the late season growth stage [-]

$K_{cb\ ini}$: basal crop coefficient during the initial growth stage [-]

$K_{cb\ mid}$: basal crop coefficient during the mid-season growth stage [-]

$K_{cb,interpolated}$: daily K_{cb} obtained by interpolation of VI-derived K_{cb} on the days of satellite overpass [-]

$K_{cb,max}$: maximum value of basal crop coefficient [-]

$K_{cb,standard}$: basal crop coefficient obtained from segmented basal crop coefficient curve determined by the values of K_{cb} at the initial, mid-season and end-season, respectively $K_{cb\ ini}$, $K_{cb\ mid}$ and $K_{cb\ end}$ [-]

$K_{cb,truth}$: basal crop coefficient assumed to be the "true" value for the interpolation analysis [-]

$K_{cb,VI}$: basal crop coefficient obtained from VI [-]

K_{cb}: basal crop coefficient [-]

K_e: soil evaporation coefficient [-]

K_r: soil evaporation reduction coefficient [-]

K_s: water stress coefficient [-]

λ: latent heat of vaporization [J kg^{-1}]

λET: latent heat flux [W m^{-2}]

NDVI: Normalized difference vegetation index [-]

P: precipitation [mm]

p: soil water depletion fraction for no stress [-]

r_a: aerodynamic resistance corresponding to ΔT [s m^{-1}]

R_n: net radiation [W m^{-2}]

RO: rainfall runoff from the soil surface [mm]

T_R: radiometric surface temperature [K]

VI: vegetation index [-]

VI_{max}: maximum vegetation index [-]

VI_{min}: minimum vegetation index [-]

Z_r: depth of the root zone [m]

$Z_{r\ max}$: maximum effective root depth [m]

$Z_{r\ min}$: effective root depth during the initial stage of crop growth [m]

ΔT: near-surface vertical temperature difference [K]

θ_{FC}: soil water content at field capacity [m^3 m^{-3}]

θ_{WP}: soil water content at the permanent wilting point [m^3 m^{-3}]

ρ_a: mean air density [kg m^{-3}]

References

Al Zayed, I.S., Elagib, N.A., Ribbe, L., Heinrich, J., 2016. Satellite-based evapotranspiration over Gezira Irrigation Scheme,Sudan: A comparative study. Agricultural Water Management, 177, 66–76. http://dx.doi.org/10.1016/j.agwat.2016.06.027

Allen, R. G., Morton, C., Kamble, B., Kilic, A., Huntington, J., Thau, D., Gorelick, N., Erickson, T., Moore, R., Trezza, R., Ratcliffe, I., Robison, C., 2015. EEFlux: A Landsat-based evapotranspiration mapping tool on the Google Earth Engine. In; Emerging Technologies for Sustainable Irrigation. A joint ASABE / IA Irrigation Symposium. Long Beach, CA, pp. 1–11.

Allen, R.G., Pereira, L.S., 2009. Estimating crop coefficients from fraction of ground cover. Irrigation Science, 28, 17–34.

Allen, R.G., Pereira, L.S., Raes, D. Smith, M., 1998. Crop evapotranspiration. Guidelines for computing crop water requirements. FAO Irrigation and Drainage Paper No. 56, Rome, Italy.

Allen, R.G., Pruitt, W.O., Raes, D., Smith, M., Pereira, L.S., 2005. Estimating evaporation from bare soil and the crop coefficient for the initial period using common soils information. Journal of Irrigation and Drainage Engineering, 131(1), 14-23.

Allen, R. G., Tasumi, M., Morse, A., Trezza, R., Wright, J. L., Bastiaanssen, W., Kramber, W.; Lorite, I., Robison, C. W., 2007a. Satellite-based energy balance for mapping evapotranspiration with internalized calibration (METRIC)—Applications. J. Irrig. Drain. Eng. ASCE 133 (4), 395-406

Allen, R.G., Tasumi, M., Trezza, R., 2007b. Satellite-based energy balance for mapping evapotranspiration with internalized calibration (METRIC)—model. J. Irrig. Drain. Eng. ASCE 133 (4), 380–394.

Angella, G., García Vila, M., López, J.M., Barraza, G., Salgado, R., Prieto Angueira, S., Tomsic, P., Fereres, E., 2016. Quantifying yield and water productivity gaps in an irrigation district under rotational delivery schedule. Irrigation Science, 34, 71–83. DOI 10.1007/s00271-015-0486-0

Angella, G., Prieto, D., Salgado, R., Salvatierra, J., Wintten, C., Coronel Lozano, A., Sarria, C., Ybarra, R., 2011. La evaluación del desempeño de los sistemas de riego como una herramienta para la mejora de su gestión. In: XXIII Congreso Nacional del Agua. ISSN 1853-7685.

Angueira, C., Zamora, E., 2007. Oeste del área de riego del Río Dulce, Santiago del Estero, Argentina. Ed. INTA. ISSN 1850 4086. Serie informes técnicos EEASE Nº40.

ASCE–EWRI, 2005. The ASCE standardized reference evapotranspiration equation. ASCE–EWRI Standardization of Reference Evapotranspiration Task Committee Rep., ASCE Reston, Va. 120 p.

Ayyad, S., Al Zayed, I.S., Ha, V.T.T., Ribbe, L., 2019. The performance of satellite-based actual evapotranspiration products and the assessment of irrigation efficiency in Egypt. Water, 11, 1913; doi:10.3390/w11091913

Bastiaanssen, W.G.M., Brito, R.A.L., Bos , M.G., Souza, R.A., Cavalcanti, E.B., Bakker, M.M., 2001. Low cost satellite data for monthly irrigation performance monitoring: benchmarks from Nilo Coelho, Brazil. Irrigation and Drainage Systems 15: 53–79.

Bastiaanssen, W.G.M., Menenti, M., Feddes, R.A., Holstlag, A.A.M., 1998. A remote sensing surface energy balance algorithm for land (SEBAL). 1. Formulation. Journal of Hydrology, 212-213, 198–212.

Bausch, W.C., Neale, C.M.U., 1987. Crop coefficients derived from reflected canopy radiation: A concept. Transactions of the ASAE, 30, 703–709.

Bausch, W.C., Neale, C.M.U., 1989. Spectral inputs improve corn crop coefficients and irrigation scheduling. Transactions of the ASAE, 32, 1901–1908.

Borgia, C., García-Bolaños, M., Li, T., Gómez-Macpherson, H., Comas, J., Connor, D., Mateos, L., 2013. Benchmarking for performance assessment of small and large irrigation schemes along the Senegal Valley in Mauritania. Agricultural Water Management, 121, 19–26.

Bos, M.G., Burton, M.A., Molden, D.J., 2005 Irrigation and drainage performance assessment –practical guidelines. CABI Publishing, Wallingford, UK, 158 pp

Calera, A., Jochum, A.M., Cuesta-Garcia, A., Montoro-Rodriguez, A., Lopez-Fuster, P., 2005. Irrigation management from space: towards user-friendly products. Irrigation and Drainage Systems, 19, 337–353.

Calera, A., Campos, I., Osann, A., D'Urso, G., Menenti, M., 2017. Remote sensing for crop water management: from ET modelling to services for the end users. Sensors, 17 (5), 1104.

Carpintero, E., Mateos, L., Andreu, A., González-Dugo, M.P., 2020. Effect of the differences in spectral response of Mediterranean tree canopies on the estimation of evapotranspiration using vegetation index-based crop coefficients. Agricultural Water Management, 238, 106201, https://doi.org/10.1016/j.agwat.2020.106201

Chalghaf, I, Elhaddad, A., García, L.A., Lecina, S., 2015. Remote sensing and district database programs for irrigation monitoring and evaluation at a regional scale. J. Irrig. Drain. Eng. ASCE 141 (11), 04015016.

Choudhury, B.J., Ahmed, N.U., Idso, S.B., Reginato, R.J., Daughtry, C.S.T., 1994. Relations between evaporation coefficients and vegetation indices studied by model simulations. Remote Sensing of the Enviroment, 50, 1–17.

Doorenbos, J., Pruitt, W.O., 1977. Crop water requirements. FAO Irrigation and Drainage Paper No.24, Rome, Italy.

D'Urso, G., Richter, K., Calera, A., Osann, M.A., Escadafal, R., Garatuza-Pajan, J., Vuolo, F., 2010. Earth observation products for operational irrigation management in the context of the PLEIADeS project. Agric. Water Manag. 98 (2), 271–282.

Droogers, P., Bastiaanssen, W., 2002. Irrigation performance using hydrological and remote sensing modeling. Journal of Irrigation and Drainage Engineering, 128 (1), 11-18.

Echevehere, P. H., 1976. Normas de reconocimiento de suelos. INTA-CIRN. Pub. N° 152 - 2° Edición. Castelar, Buenos Aires.

Elhaddad, A., Garcia, L. A., 2011. Surface energy balance model for calculating evapotranspiration using a raster approach. Journal of Irrigation and Drainage Engineering, 137 (4), 203–210.

Elhaddad, A., Garcia, L. A., 2014. Using a surface energy balance model (ReSET-Raster) to estimate seasonal crop water use for large agricultural areas: Case study of the Palo Verde irrigation district. Journal of Irrigation and Drainage Engineering, 140 (10), 05014006.

Er-Raki, S., Chehbouni, A., Duchemin, B., 2010. Combining satellite remote sensing data with the fao-56 dual approach for water use mapping in irrigated wheat fields of a semi-arid region. Remote Sensing, 2, 375-387. doi:10.3390/rs2010375

Foolad, F., Blankenau, P., Kilic, A., Allen, R. G., Huntington, J. L., Erickson, T. A., Ozturk, D., Morton, C. G., Ortega, S., Ratcliffe, I., Franz, T. E., Thau, D., Moore, R., Gorelick, N., Kamble, B., Revelle, P., Trezza, R., Zhao, W., Robison, C. W., 2018. Comparison of the Automatically Calibrated Google Evapotranspiration Application—EEFlux and the Manually Calibrated METRIC Application. doi: 10.20944/preprints201807.0040.v1

French, A.N., Hunsaker, D.J., Bounoua, L., Karnieli, A., Luckett, W.E., Strand, R., 2018. Remote Sensing of Evapotranspiration over the Central Arizona Irrigation and Drainage District, USA. Agronomy, 8, 278. doi:10.3390/agronomy8120278

French, A.N., Hunsaker, D.J., Thorp, K.R., 2015. Remote sensing of evapotranspiration over cotton using the TSEB and METRIC energy balance models. Remote Sensing of Environment 158, 281–294.

Galizzi, F., González, C., Nazar, P., Elias Tissera, N. J., Ramírez, N. M., Gómez, N. A., 2015. Condición inicial de un suelo degradado por el uso agrícola continuado en la zona IV de riego del Rio Dulce (Provincia de Santiago del Estero). X Jornadas de Ciencia y Tecnología de Facultades de Ingeniería del NOA. Salta 21 al 22 de mayo de 2015.

Gibson, K.E.B., Yang, H.S., Franz, T., Eisenhauer, D., Gates, J.B., Nasta, P., Farmaha, B.S., Grassini, P., 2018. Assessing explanatory factors for variation in on-farm irrigation in US maize-soybean systems. Agricultural Water Management, 197, 34–40

Gonzalez-Dugo, M. P., Escuin, S., Cano, F., Cifuentes, V., Padilla, F.L.M., Tirado, J.L., Oyonarte, N., Fernández, P., Mateos, L., 2013. Monitoring evapotranspiration of irrigated crops using crop coefficients derived from time series of satellite images. II. Application on basin scale. Agricultural Water Management, 125, 92– 104.

González-Dugo, M.P., Mateos, L., 2008. Spectral vegetation indices for benchmarking water productivity of irrigated cotton and sugarbeet crops. Agricultural Water Management, 95, 48–58.

Gonzalez-Dugo, M.P., Neale, C.M.U., Mateos, L., Kustas, W.P., Prueger, J.H., Anderson, M.C., Li., F., 2009. A comparison of operational remote sensing-based models for estimating crop evapotranspiration. Agricultural and Forest Meteorology, 149, 1843–1853.

He, R., Jin, Y., Kandelous, M.M., Zaccaria, D., Sanden, B.L., Snyder, R.L., Jiang, J., Hopmans, J.W., 2017. Evapotranspiration estimate over an almond orchard using Landsat satellite observations. Remote Sensing, 9, 436. doi:10.3390/rs9050436

Huete, A.R., Jackson, R.D., Post, D.F., 1985. Spectral response of a plant canopy with different soil background. Remote Sensing of the Environment, 17, 37–53.

Irmak, A., Allen, R.G., Kjaersgaard, J., Huntington, J., Kamble, B., Trezza, R., Ratcliffe, I., 2012. Operational Remote Sensing of ET and Challenges, Evapotranspiration - Remote Sensing and Modeling, Dr. Ayse Irmak (Ed.), ISBN: 978-953-307-808-3, InTech, Available from: https://www.intechopen.com/books/evapotranspiration-remote-sensing-and-modeling/operational-remote-sensing-of-et-and-challenges

Kustas, W.P., Norman, J.M., 1996. Use of remote sensing for evapotranspiration monitoring over land surfaces. Hydrological Sciences, 41, 495–516.

López-Urrea, R., Martín de Santa Olalla, F., Montoro, A., López-Fuster, P., 2009. Single and dual crop coefficients and water requirements for onion (Allium cepa L.) under semiarid conditions. Agricultural Water Management, 96, 1031–1036.

Lozano, D., Mateos, L., 2008. Usefulness and limitations of decision support systems for improving irrigation scheme management. Agricultural Water Management, 95, 409–418

Malano, H., Burton, M., 2001. Guidelines for benchmarking performance in the irrigation and drainage sector. International Programme for Technology and Research in Irrigation and Drainage, FAO, Rome, 43 pp

Malano, H., Burton, M., Makin, I., eds., 2004. Benchmarking of irrigation and drainage sectors. Irrigation and Drainage, 53(2), 214 pp

Mateos, L., González-Dugo, M.P., Testi, L., Villalobos, F.J., 2013. Monitoring evapotranspiration of irrigated crops using crop coefficients derived from time series of satellite images. I. Method validation. Agricultural Water Management, 125, 81–91.

Melton, F.S., Johnson, L.F., Lund, C.P., Pierce, L.L., Michaelis, A.R., Hiatt, S.H., Guzman,A., Adhikari, D., Purdy, A.J., Rosevelt, C., Votava, P., Trout, T.J., Temesgen, B., Frame, K., Sheffner, E.J., Nemani, R.R., 2012. Satellite irrigation management support with the terrestrial observation and prediction system: A framework for integration of satellite and surface observations to support improvements in agricultural water resource management. IEEE Journal of Selected Topics in Applied Earth Observations and Remote Sensing,5, 1709-1721.

Menenti, M., Visser, T.N.M., Morabito, J.A., Drovandi, A., 1989. Appraisal of irrigation performance with satellite data and georeferenced information, in Rydzewski, J.R. and Ward, C.F. (eds.) Irrigation, Theory and Practice, Proc. of the Int. Conf., Institute of Irrigation Studies, Southampton, 12–15 September 1989: 785–801. Pentech Press, London.

Molden, D., Sakthivadivel, R., Perry, C.J., de Fraiture, C., Kloezen, W.H., 1998. Indicators for comparing performance of irrigated agricultural systems. Research Report No 20. International Water Management Institute, Colombo, Sri Lanka, 26 pp.

Morábito, J., Bos, M., Vos, S., Brouwer, R., 1998. The quality of service provided by the irrigation department to the users associations, Tunuyán System, Mendoza, Argentina. Irrigation and Drainage System, 12, 49-65.

Morello, J., Adámoli, J., 1974. Las grandes unidades de vegetación y ambiente del Chaco argentino. Segunda parte. Vegetación y ambiente de la provincia del Chaco. La vegetación de la República Argentina, Serie Fitogeográfica, 13, 130.

Neale, C.M.U., Bausch, W.C., Heermann, D.F., 1989. Development of reflectance based crop coefficients for corn. Transactions of the ASAE 32, 1891–1899.

NRCS Nacional Engineering Handbook, 2004. Part 630 Hydrology. Chapter 10. Estimation of Direct Runoff from Storm Rainfall. US Department of Agriculture, Natural Resources Conservation Service.

Paço, T.A., Pôças, I., Cunha, M., Silvestre, J.C., Santos, F.L., Paredes, P., Pereira, L.S., 2014. Evapotranspiration and crop coefficients for a super intensive olive orchard. An application of SIMDualKc and METRIC models using ground and satellite observations. Journal of Hydrology, 519, 2067–2080.

Pereira, L.S., Paredes, P., Hunsaker, D.J., López-Urrea, R., Mohammadi Shad, Z., 2020a. Standard single and basal crop coefficients for field crops. Updates and advances to the FAO56 crop water requirements method. Agric. Water Manage.

Pereira, L.S., Paredes, P., López-Urrea, R., Hunsaker, D.J., Mota, R.M., Mohammadi Shad, Z., 2020b. Standard single and basal crop coefficients for vegetable crops, an update of FAO56 crop water requirements approach. Agric. Water Manage.

Pôças, I., Calera, A., Campos, I., Cunha, M., 2020. Remote sensing for estimating and mapping single and basal crop coefficients: a review on spectral vegetation indices approaches. Agricultural Water Management Volume 233,106081, https://doi.org/10.1016/j.agwat.2020.106081

Pôças, I., Paço, T.A., Paredes, P., Cunha, Pereira, L.S., 2015. Estimation of actual crop coefficients using remotely sensed vegetation indices and soil water balance modelled data. Remote Sensing, 7, 2373-2400. doi:10.3390/rs70302373

QGIS Development Team (2019). QGIS Geographic Information System. Open Source Geospatial Foundation Project. http://qgis.osgeo.org

Rawles, W. J., Brakensiek, D. L., 1982. Estimating soil water retention from soil properties. Journal of the Irrigation and Drainage Division, ASCE, 108(2), 166-171.

Rodríguez-Díaz, J.A., Camacho-Poyato, E., López-Luque, R., Pérez-Urrestarazu, L., 2008. Benchmarking and multivariate data analysis techniques for improving the efficiency of irrigation districts: an application in Spain. Agricultural Systems 96, 250–259.

Roerink, G. J., Bastiaanssen, W. G. M., Chambouleyron, J., Menenti, M., 1997. Relating crop water consumption to irrigation water supply by remote sensing. Water Resources Management, 11, 445–465.

Santos, C., Lorite, I.J., Tasumi, M., Allen, R.G., Fereres, E., 2008. Integrating satellite-based evapotranspiration with simulation models for irrigation management at the scheme level. Irrigation Science, 26, 277–288. DOI 10.1007/s00271-007-0093-9

Segovia-Cardozo, D.A., Rodríguez-Sinobas, L., Zubelzu, S., 2019. Water use efficiency of corn among the irrigation districts across the Duero river basin (Spain): Estimation of local crop coefficients by satellite images. Agricultural Water Management, 212, 241–251.

Simonneaux, V., Duchemin B., Helson, D., Er-Raki, S., Olioso, A., Chehbouni, A.G., 2008. The use of high-resolution image time series for crop classification and evapotranspiration estimate over an irrigated area in central Morocco, International Journal of Remote Sensing, 29, 95-116. doi: 10.1080/01431160701250390

Taghvaeian, S., Neale, C.M.U., 2011. Water balance of irrigated areas: a remote sensing approach. Hydrological Processes, 25, 4132–4141. DOI: 10.1002/hyp.8371

Taghvaeian, S., Neale, C. M., Osterberg, J. C., Sritharan, S. I., Watts, D. R., 2018. Remote sensing and GIS techniques for assessing irrigation performance: Case study in

Southern California. Journal of Irrigation and Drainage Engineering, 144 (6), 05018002.

Tasumi, M., Allen, R.G., 2007. Satellite-based ET mapping to assess variation in ET with timing of crop development. Agricultural Water Management, 88, 54–62.

Tasumi, M., Allen, R.G., Trezza, R., Wright, J.L., 2005. Satellite-based energy balance to assess within-population variance of crop coefficient curves. Journal of Irrigation and Drainage Engineering, 131, 94-109.

Zema, D.A., Nicotra, A., Mateos, L., Zimbone, S.M., 2018, Improvement of the irrigation performance in Water Users Associations integrating data envelopment analysis and multi-regression models. Agricultural Water Management, 205, 38–49 https://doi.org/10.1016/j.agwat.2018.04.032.

Zhang, H., Anderson, R.G., Wanga, D., 2015. Satellite-based crop coefficient and regional water use estimates for Hawaiian sugarcane. Field Crops Research, 180, 143–154.

Caption to figures

Figure 1. Location of the study case Río Dulce irrigation scheme (Santiago del Estero, Argentina), the selected irrigation subsystems (El Alto and APAZ-IV), the selected crops fields, the two weather stations used in the study.

Figure 2. Segmented curve for the standard basal crop coefficient ($K_{cb,standard}$), mean VI-derived basal crop coefficient obtained from VI ($K_{cb,VI}$) for the dates of overpass satellites for cotton (a) and alfalfa (c). Segmented curve for the standard crop coefficient ($K_{c,standard}$), synthetic crop coefficient on the dates of satellite overpass and daily synthetic crop coefficient for cotton (b) and alfalfa (d). Averages are of 84 and 161 cotton crops fields and 42 and 1344 alfalfa crops fields in the El Alto and APAZ-IV subsystems, respectively, in season 2014-15. Vertical bars indicate standard deviations.

Figure 3. Relationship between evapotranspiration estimated with the synthetic crop coefficient ($ET_{c,synthetic}$) and obtained using $K_{cb,VI}$ and computing K_s and K_e running a water balance for a given irrigation schedule and ($ET_{c,VIact}$) for the 30 selected crops fields in APAZ-IV in the season 2014-15. Triangles represent maize fields (7) and circles represent cotton fields (23).

Figure 4.Relationship between crop coefficients obtained from EEFlux ($K_{c,EEFlux}$) and the corresponding a) crop coefficient ($K_{c,VIact}$) obtained from $K_{cb,VI}$ and computing K_s and K_e running a water balance for a given irrigation schedule or b) synthetic crop coefficients($K_{c,synthetic}$). Triangles represent maize fields and circles cotton fields on dates of overpass satellite in season 2014-15.

Figure 5. Relationship between reference evapotranspiration provided by EEFlux ($ET_{o,EEFlux}$) and recorded at the INTA weather station ($ET_{o,INTA}$) on dates of satellite overpass in the years 2014-18.

Figure 6. Evolution of $K_{c,truth}$, $K_{cb,truth}$, $K_{cb,interpolated}$, $K_{c,synthetic}$, and $K_{c,interpolated}$ in the interpolation simulation analysis for season 2014-15 and satellite overpass intervals of 15 (a) and 35 (b) days. Satellite overpass dates are indicated by diamonds. The simulation analysis was carried out for a cotton crop in the conditions of APAZ-IV.

Figure 7. Root Mean Square Error (RMSE) of daily ET_c obtained from $K_{c,interpolated}$ and $K_{c,synthetic}$ with respect to the "truth" value as a function of the hypothetical interval of satellite overpass and assuming full irrigation strategy. The simulation analysis was

carried out for a cotton crop in the conditions of APAZ-IV and 30 climate years (July 1, 1988 - June 30, 2018). The vertical bars indicate the standard deviation.

Figure 8. Relative Error (RE) of seasonal ET_c obtained from $K_{c,interpolated}$ and $K_{c,synthetic}$ with respect to the "truth" value as a function of the hypothetical interval of satellite overpass and assuming full (a) and deficit (b) irrigation strategy. The simulation analysis was carried out for a cotton crop in the conditions of APAZ-IV and 30 climate years (July 1, 1988 - June 30, 2018). The vertical bars indicate the standard deviation.

Figure 9. Seasonal ET_c in 30 selected crop fields obtained by interpolating K_c derived from actual and reference evapotranspiration provided by EEFlux on days of satellite overpass represented against: a) ET_c derived from interpolation of $K_{cb,VI}$ on the days of satellite overpass and computing K_s and K_e running a water balance for a given irrigation schedule and b) ET_c derived from the synthetic crop coefficient method. In a) and b), the reference evapotranspiration was recorded at the INTA weather station. The crops were maize and cotton in APAZ-IV grown in the season 2014-15.

Figure 10. Evolution of $K_{cb,VI}$, $K_{c,VIact}$, $K_{c,interpolated}$ from EEFlux (obtained by interpolating K_c derived from actual and reference evapotranspiration provided by EEFlux) and $K_{c,synthetic}$, in a cotton field (a) and a maize field (b) from the 30 crop fields selected in APAZ-IV in the season 2014-15. Satellite overpass dates are indicated by diamonds.

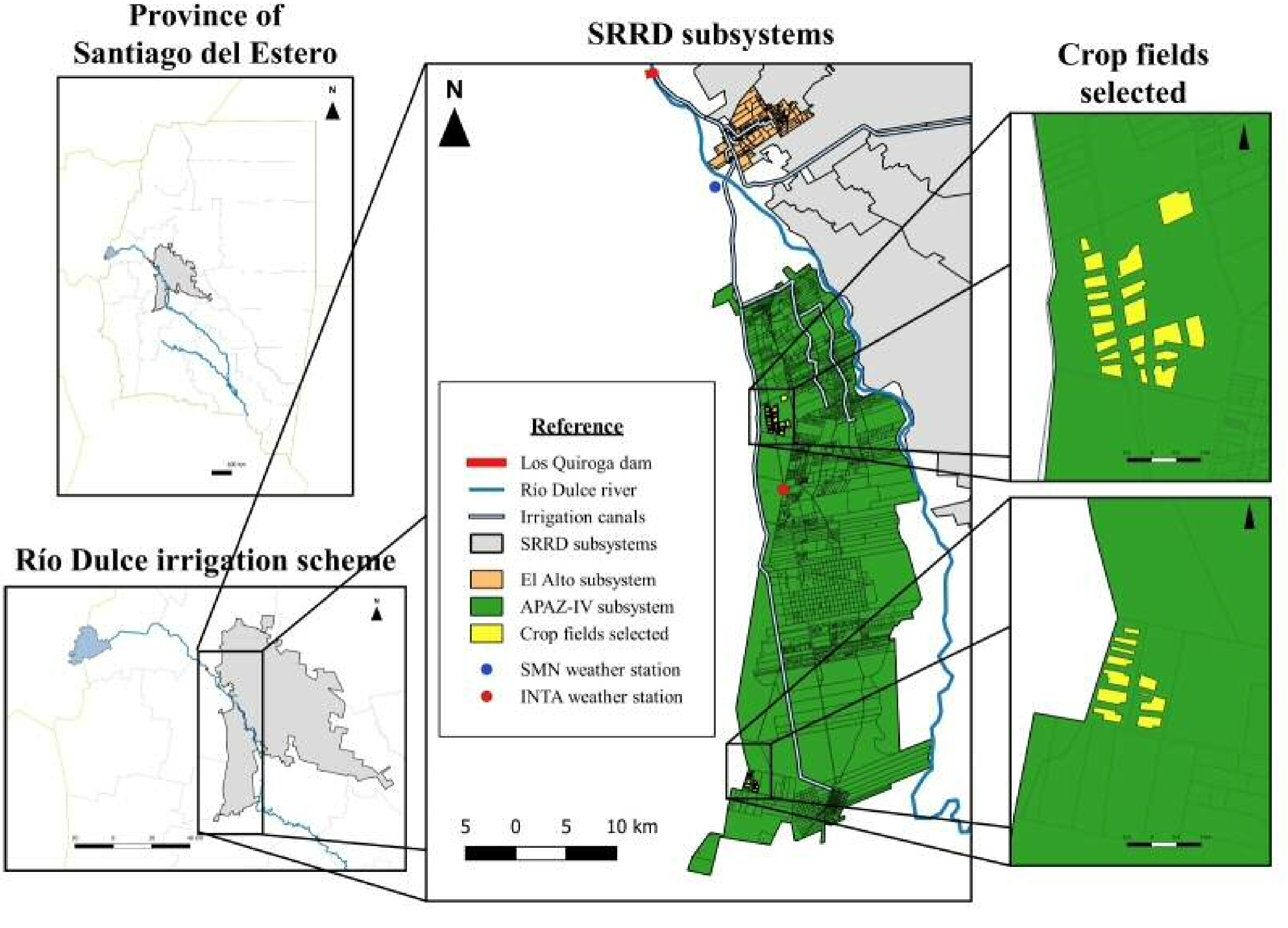
Province of
Santiago del Estero
SRRD subsystems
Crop fields
selected
Río Dulce irrigation scheme
N
Reference
Los Quiroga dam
Río Dulce river
Irrigation canals
SRRD subsystems
El Alto subsystem
APAZ-IV subsystem
Crop fields selected
SMN weather station
INTA weather station
5 0 5 10 km

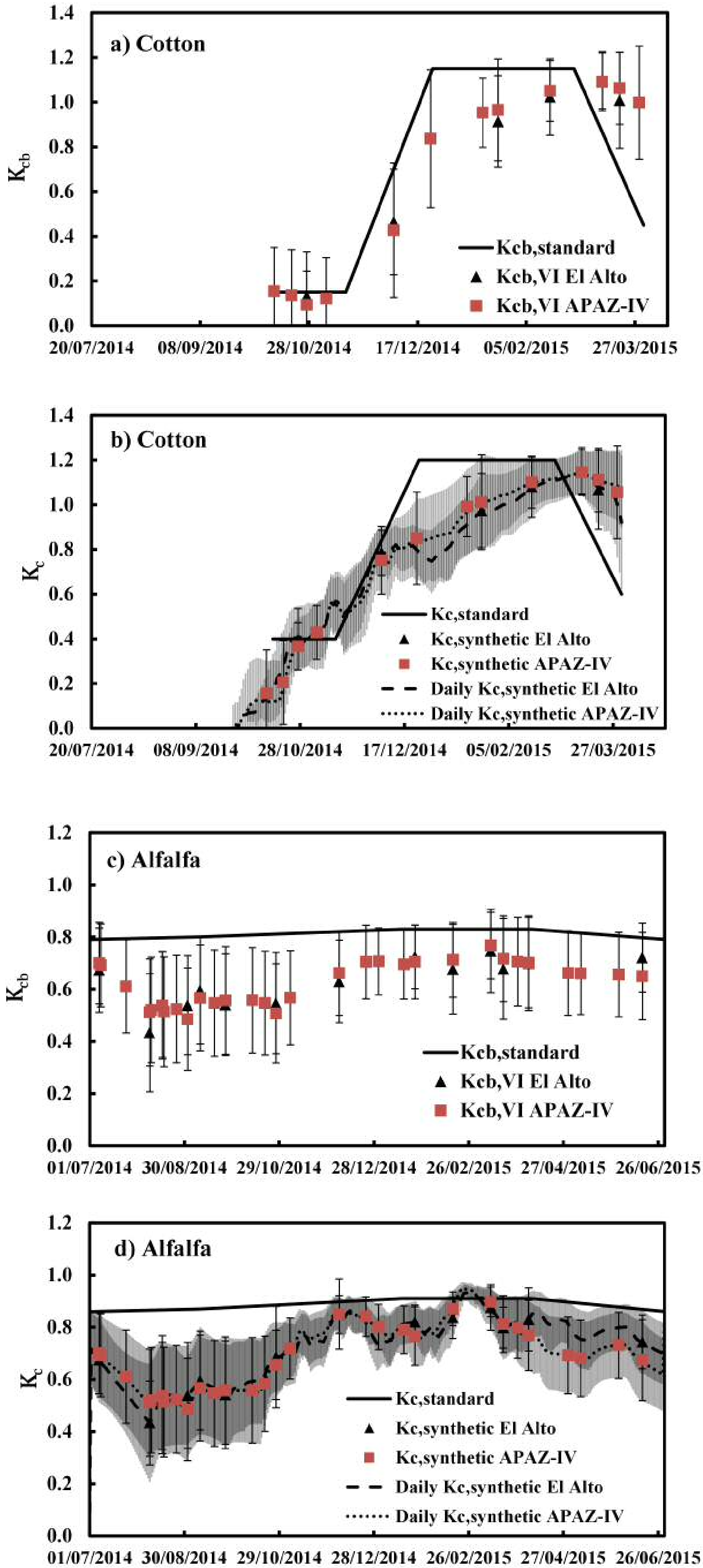
a) Cotton
Kcb
Kcb,standard
Kcb,VI El Alto
Kcb,VI APAZ-IV
20/07/2014
08/09/2014
28/10/2014
17/12/2014
05/02/2015
27/03/2015
b) Cotton
Kc
Kc,standard
Kc,synthetic El Alto
Kc,synthetic APAZ-IV
Daily Kc,synthetic El Alto
Daily Kc,synthetic APAZ-IV
c) Alfalfa
Kcb
Kcb,standard
Kcb,VI El Alto
Kcb,VI APAZ-IV
01/07/2014
30/08/2014
29/10/2014
28/12/2014
26/02/2015
27/04/2015
26/06/2015
d) Alfalfa
Kc
Kc,standard
Kc,synthetic El Alto
Kc,synthetic APAZ-IV
Daily Kc,synthetic El Alto
Daily Kc,synthetic APAZ-IV

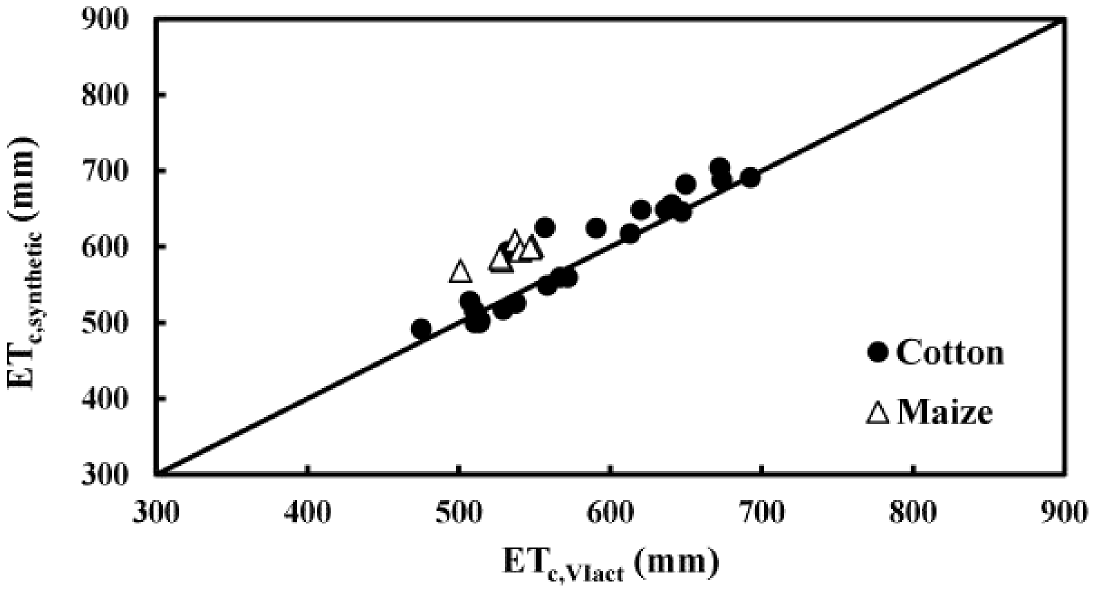

900
800
700
600
500
400
300
300
400
500
600
700
800
900
$ET_{c,synthetic}$ (mm)
$ET_{c,VIact}$ (mm)
Cotton
Maize

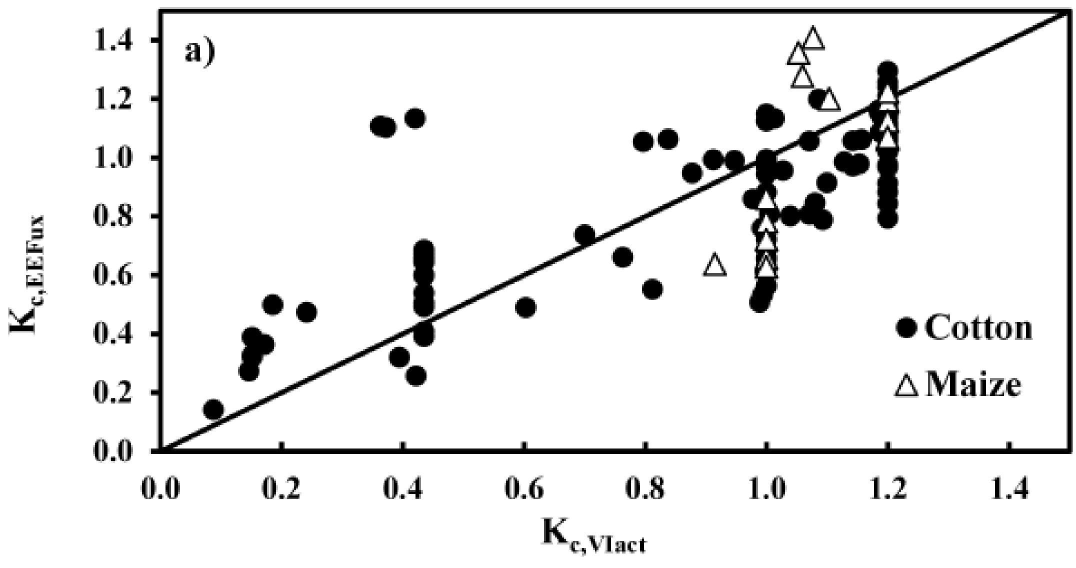
a)
Kc,EEFux
Kc,VIact
● Cotton
△ Maize
0.0
0.2
0.4
0.6
0.8
1.0
1.2
1.4

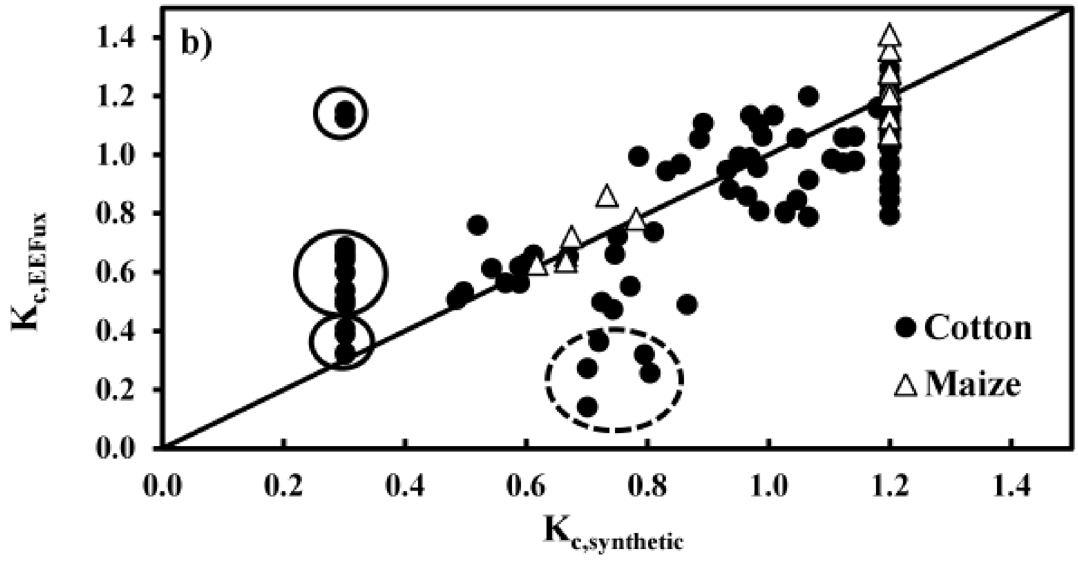
b)
Kc,EEFux
Kc,synthetic
● Cotton
△ Maize
0.0
0.2
0.4
0.6
0.8
1.0
1.2
1.4

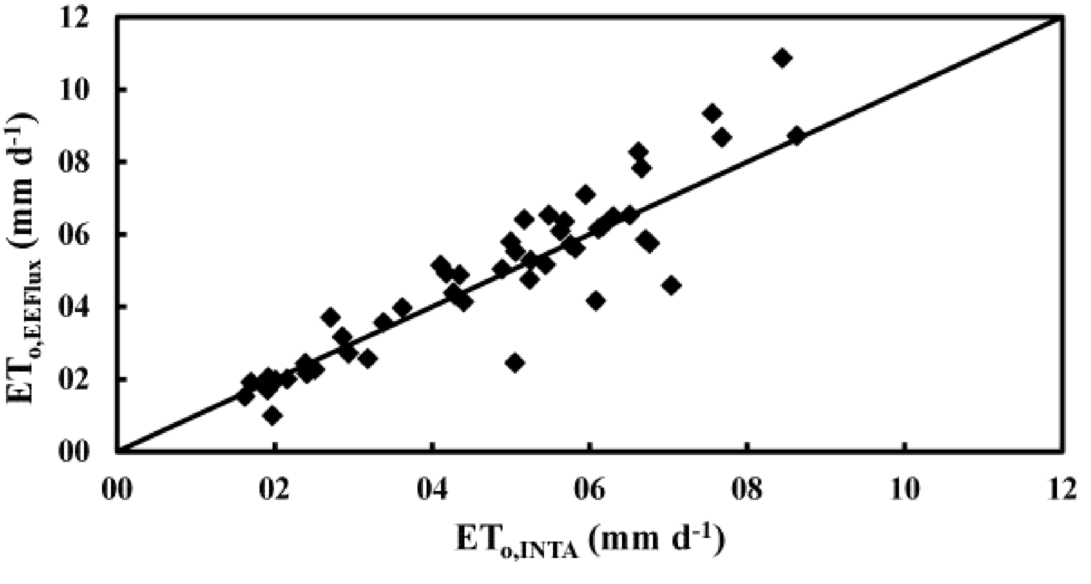
12
10
08
06
04
02
00
ET$_{o,EEFlux}$ (mm d^{-1})
00
02
04
06
08
10
12
ET$_{o,INTA}$ (mm d^{-1})

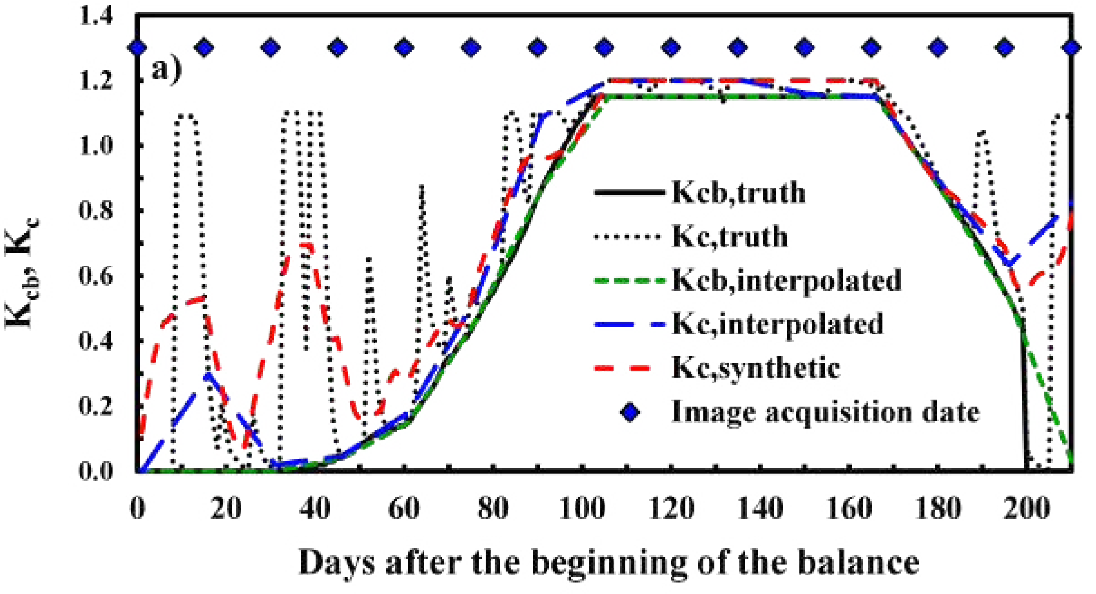
1.4
1.2
1.0
0.8
0.6
0.4
0.2
0.0
a)
K_{cb}, K_c
Kcb,truth
Kc,truth
Kcb,interpolated
Kc,interpolated
Kc,synthetic
Image acquisition date
0
20
40
60
80
100
120
140
160
180
200
Days after the beginning of the balance

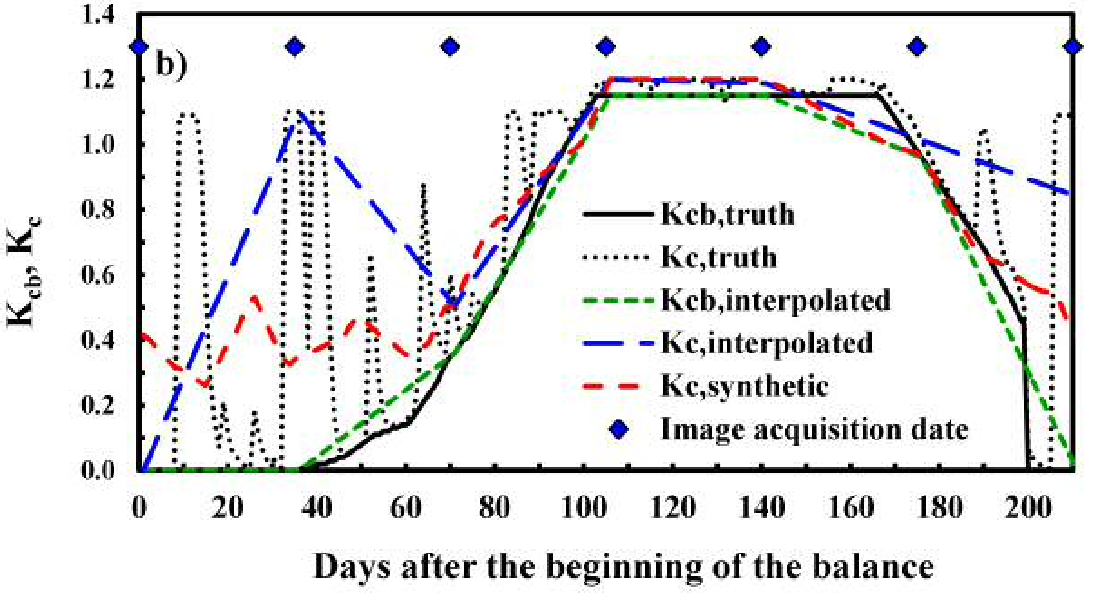
1.4
1.2
1.0
0.8
0.6
0.4
0.2
0.0
b)
K_{cb}, K_c
Kcb,truth
Kc,truth
Kcb,interpolated
Kc,interpolated
Kc,synthetic
Image acquisition date
0
20
40
60
80
100
120
140
160
180
200
Days after the beginning of the balance

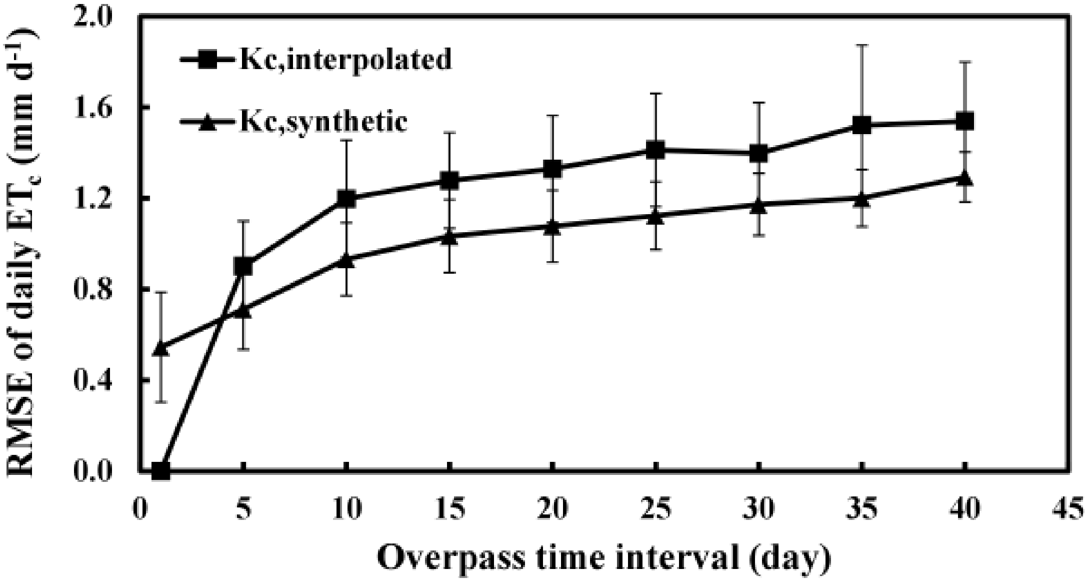
Kc,interpolated
Kc,synthetic
RMSE of daily ET_c (mm d^{-1})
Overpass time interval (day)
2.0
1.6
1.2
0.8
0.4
0.0
0
5
10
15
20
25
30
35
40
45

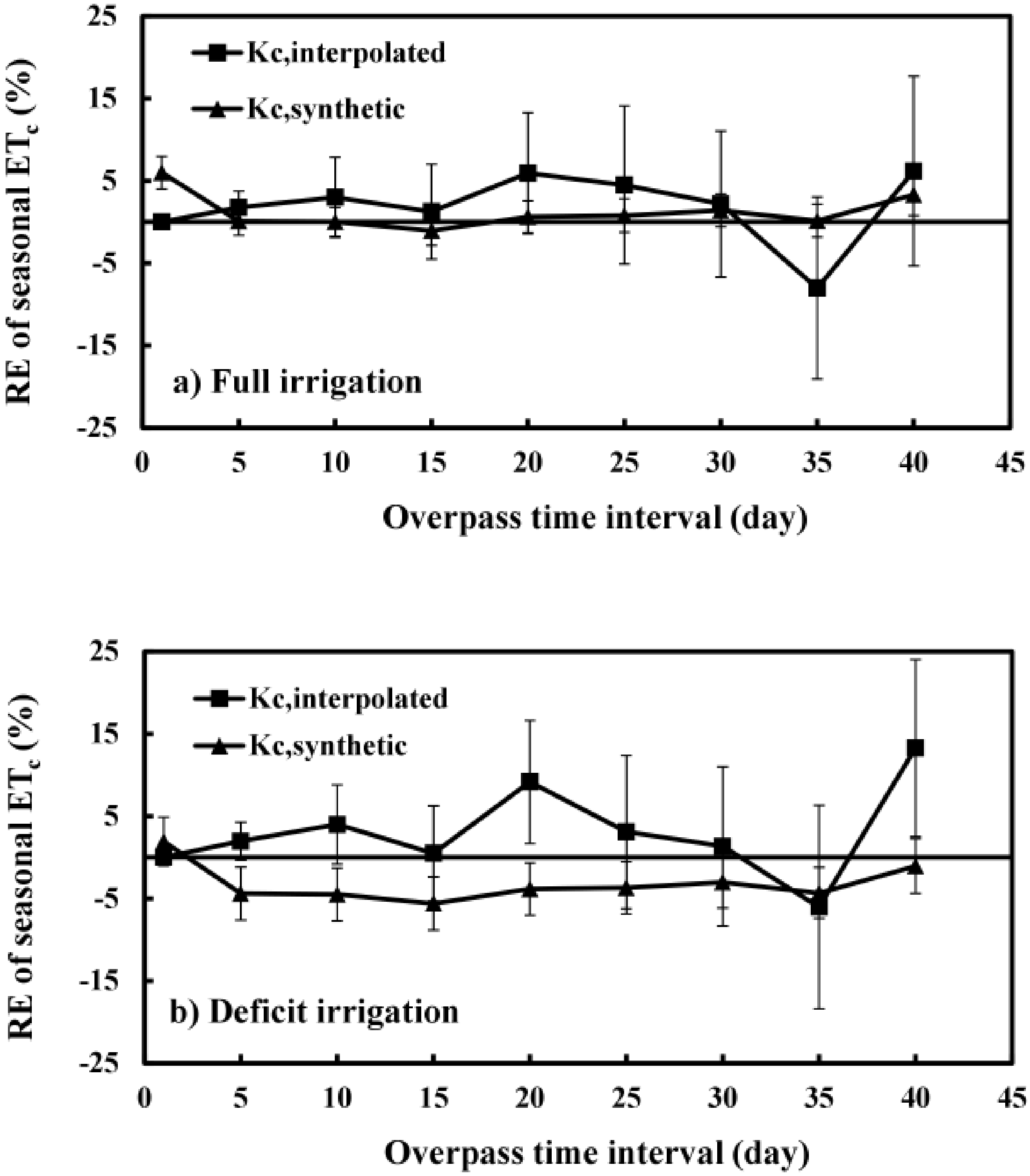

25
15
5
-5
-15
-25
RE of seasonal ET_c (%)
Kc,interpolated
Kc,synthetic
a) Full irrigation
0 5 10 15 20 25 30 35 40 45
Overpass time interval (day)
b) Deficit irrigation

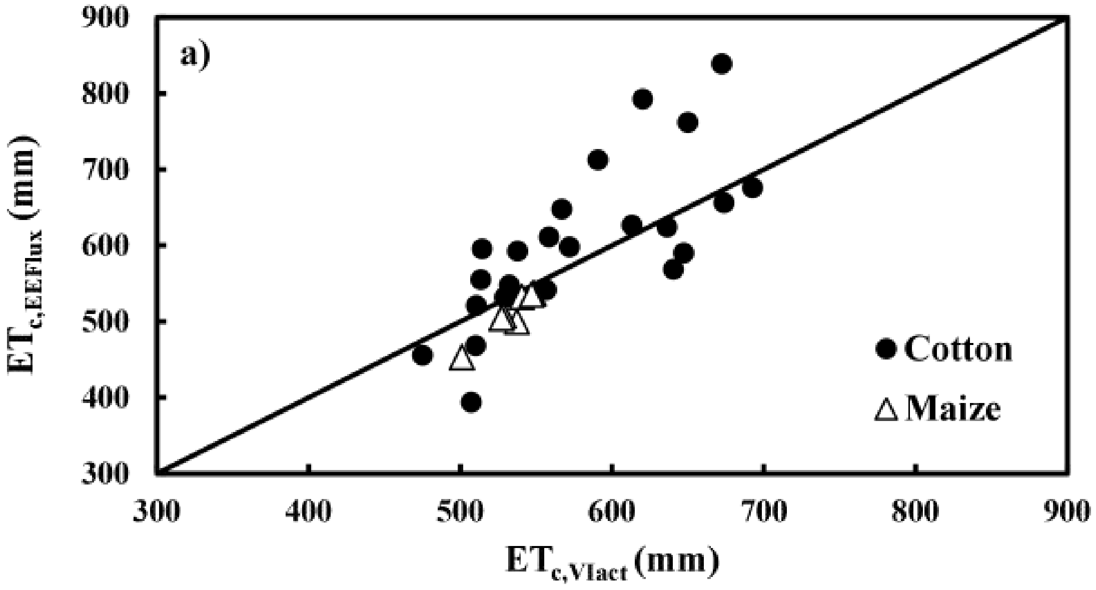
a)
900
800
700
600
500
400
300
300
400
500
600
700
800
900
$ET_{c,EEFlux}$ (mm)
$ET_{c,VIact}$ (mm)
Cotton
Maize

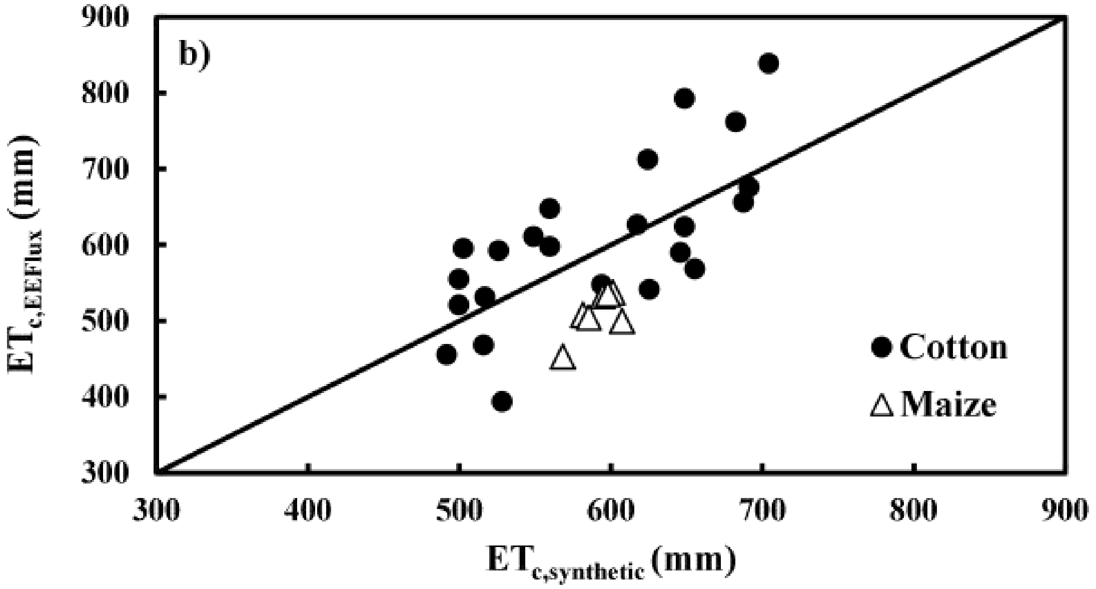
b)
900
800
700
600
500
400
300
300
400
500
600
700
800
900
$ET_{c,EEFlux}$ (mm)
$ET_{c,synthetic}$ (mm)
Cotton
Maize

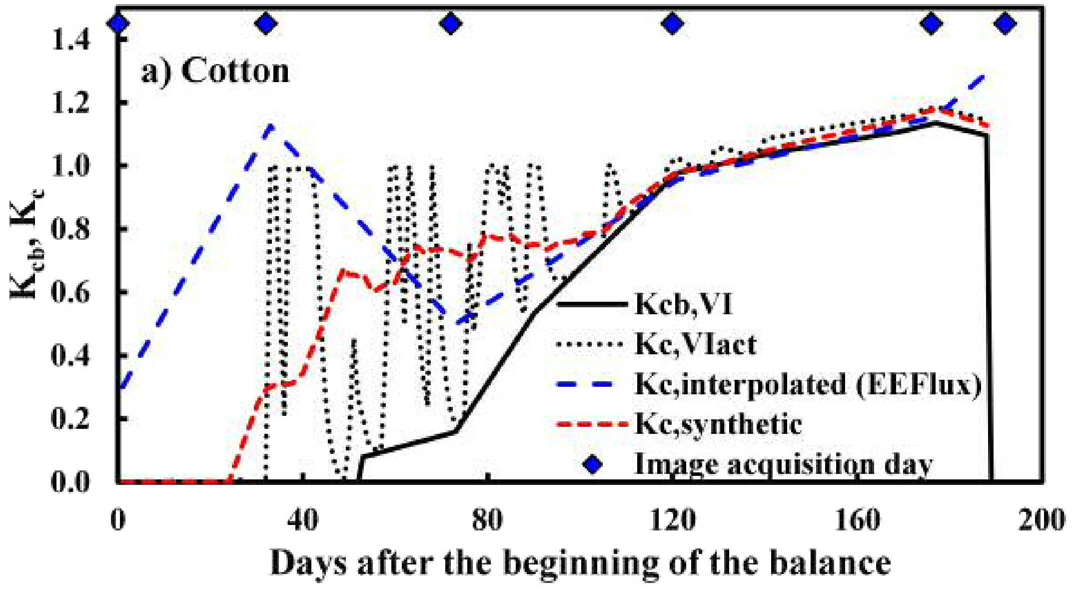
a) Cotton
Kcb, Kc
1.4
1.2
1.0
0.8
0.6
0.4
0.2
0.0
0
40
80
120
160
200
Days after the beginning of the balance
Kcb,VI
Kc,VIact
Kc,interpolated (EEFlux)
Kc,synthetic
Image acquisition day

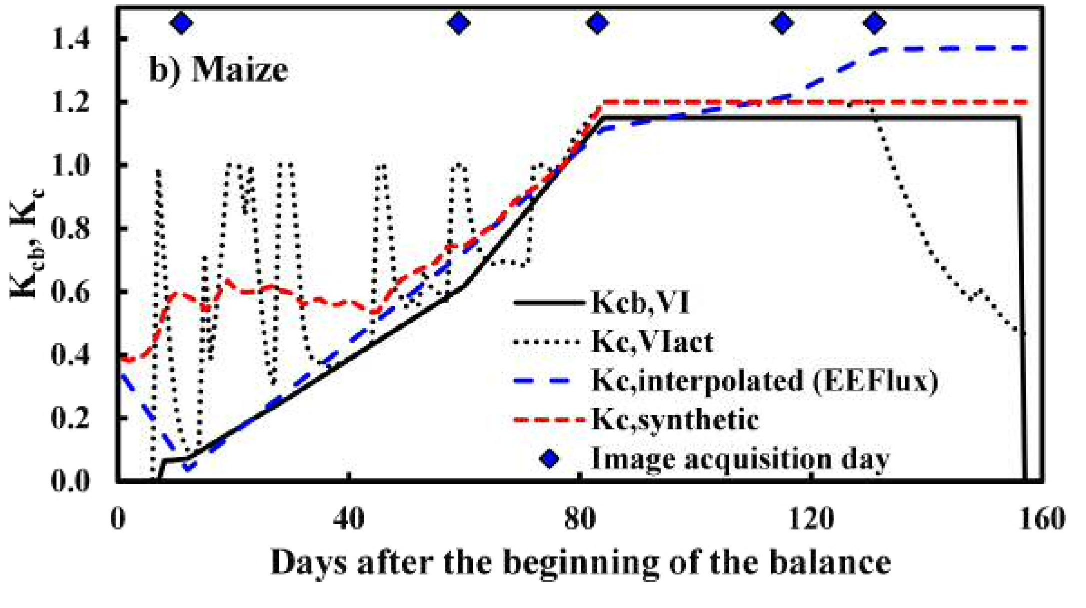
b) Maize
Kcb, Kc
1.4
1.2
1.0
0.8
0.6
0.4
0.2
0.0
0
40
80
120
160
Days after the beginning of the balance
Kcb,VI
Kc,VIact
Kc,interpolated (EEFlux)
Kc,synthetic
Image acquisition day

Table 1. Properties of the typical soil profile of soil classes El Simbol and La María in the study area (Angueira and Zamora, 2007).

Soil class	Layer	Thicknes (mm)	Sand (%)	Silt (%)	Clay (%)	Texture	Water content at saturation (%)	Water holding capacity (mm m^{-1})	Electrical conductivity (dSm m^{-1})	pH	Organic matter (%)
El Simbol	A	220	25	58	17	Silty loam	48	200	0.58	7.0	3.22
	B2t	310	22	60	18	Silty loam	43	180	0.46	7.2	1.55
	B3	370	19	64	17	Silty loam	44	180	0.62	7.7	1.00
	C1	>900	50	45	5	Silty loam	35	130	0.58	7.9	0.21
La María	A	200	24	64	12	Silty loam	39	200	0.5	6.3	2.39
	AC	320	28	62	10	Silty loam	36	180	0.2	7.2	1.14
	C1ca	350	31	58	11	Silty loam	32	160	0.9	7.8	0.53
	C2ca	>870	34	60	6	Silty loam	39	170	3.5	7.9	1.16

Table 2. Series of images of satellites Landsat 7 and Landsat 8 used from EEFlux plataform.

Path/Row	Satellite	Date	Path/Row	Satellite	Date
230/79-230/80	Landsat 7	07/07/14	229/80	Landsat 8	16/01/15
229/80	Landsat 8	08/07/14	230/79	Landsat 8	23/01/15*
229/80	Landsat 8	24/07/14	230/79-230/80	Landsat 7	16/02/15*
230/79-230/80	Landsat 7	08/08/14	230/79	Landsat 8	12/03/15*
229/80	Landsat 8	09/08/14	230/79-230/80	Landsat 7	20/03/15*
230/79	Landsat 8	16/08/14	229/80	Landsat 7	29/03/15
229/80	Landsat 7	17/08/14	230/79-230/80	Landsat 7	05/04/15*
229/80	Landsat 8	25/08/14	229/80	Landsat 7	30/04/15
230/79	Landsat 8	01/09/14*	229/80	Landsat 8	08/05/15
230/79-230/80	Landsat 7	09/09/14*	229/80	Landsat 7	01/06/15
229/80	Landsat 7	18/09/14	230/79	Landsat 8	16/06/15*
230/79-230/80	Landsat 7	25/09/14*			
229/80	Landsat 8	12/10/14			
229/80	Landsat 7	20/10/14			
230/79-230/80	Landsat 7	27/10/14*			
229/80	Landsat 7	05/11/14			
230/79	Landsat 8	06/12/14*			
229/80	Landsat 7	23/12/14			
229/80	Landsat 8	31/12/14			

Path/row 230/79 includes the entire subsystems under analysis.
*Dates used to obtain $ET_{c,EEFlux}$ and ET_o for the analysis of the 30 selected fields.

Table 3. Area and number of fields for each crop in the study area, crop parameters used for computing evapotranspiration using the FAO56 standard procedure and from VI-derived crop coefficients. $K_{cb,standard}$: standard basal crop coefficient; $K_{c,standard}$: standard crop coefficient; $Z_{r\ max}$: maximum effective root depth; $f_{c,Kcbmax}$: fraction of soil surface covered by vegetation for maximum K_{cb} value; $NDVI_{max}$ and $NDVI_{min}$: the Normalized Difference Vegetation Index maximum and minimum, respectively; p: soil water depletion fraction for no stress.

Parameter		Alfalfa	Cotton	$Maize_1$	$Maize_2$	Soybean	Onion	Melon	Water-melon	Oat
Total area (ha)		4353	2418	271	215	517	175	48	3	5
Number of fields		1386	245	18	20	8	40	20	4	2
Start of analysis (dd/mm)		01/07	25/09	25/11	01/07	25/11	15/02	01/07	01/07	15/04
Sowing date (dd/mm)*		01/07	15/10	01/12	01/10	01/12	15/02	15/08	01/10	15/04
Harvest date (dd/mm)*		30/06	31/03	30/04	20/01	30/04	15/10	15/12	15/11	21/10
Growth Stages (days)*										
	Initial	70[3]	30	20	20	20	45	20	20	30
	Develop.	128[3]	40	45	30	40	50	30	30	45
	Mid-season	123[3]	65	50	40	65	50	25	30	75
	Late season	44[3]	32	35	21	25	85	17	10	40
$K_{cb,standard}$[1]										
	Initial	0.79[4]	0.15	0.15	0.15	0.15	0.15	0.15	0.15	0.15
	Mid-season	0.83[4]	1.15	1.15	1.15	1.10	0.90	1.00	0.95	1.10
	Late season	0.80[4]	0.50	0.15	0.15	0.30	0.90	0.70	0.70	0.15
$K_{c,standard}$[1]										
	Initial	0.87[4]	0.40	0.52[a]/0.60[b]	0.30[a]/0.35[b]	0.52[a]/0.60[b]	0.83	0.10[a]/0.15[b]	0.30[a]/0.35[b]	0.45[a]/0.30[b]
	Mid-season	0.91[4]	1.20	1.20	1.20	1.15	1.00	1.05	1.00	1.15
	Late season	0.86[4]	0.70	0.35	0.35	0.50	1.00	0.75	0.75	0.25
$Z_{r\ max}$ (m)[1]		2.00[5]	1.50[5]	1.30	1.30	1.30	0.50	1.00	1.00	1.00
$f_{c,Kcbmax}$[2]		0.80	0.80	0.80	0.80	0.80	0.80	0.80	0.80	0.80
$NDVI_{max}$[2]		0.90	0.90	0.90	0.90	0.90	0.90	0.90	0.90	0.90
$NDVI_{min}$		0.15	0.15	0.15	0.15	0.15	0.15	0.15	0.15	0.15
p[1]		0.55	0.65	0.50	0.50	0.50	0.30	0.45	0.40	0.55

$Maize_1$: maize growing in summer; $Maize_2$: maize growing in spring.

[*] Dates representing typical growing practices in SRRD. These dates were used only to depict the standard crop coefficients.
[a] For El Alto subsystem.
[b] For APAZ-IV subsystem.
[1]FAO56 manual
[2]Gonzalez-Dugo et al. (2009)
[3]Values for the periods of winter, spring-summer, summer-autumn and autumn-winter, respectively, in SRRD.
[4]Average values for the local cutting periods in each growth phases along the season.
[5]Values based on experiences of local extension agents and INTA agronomists.

Table 3. $ET_{c,standard}$, $ET_{c,VIopt}$ and $ET_{c,synthetic}$ of each subsystem in season 2014-15.

Subsystem	$\mathbf{ET_{c,standard}}$ (mm)	$\mathbf{ET_{c,VIopt}}$ (mm)	$\mathbf{ET_{c,synthetic}}$ (mm)
El Alto	843	720	702
APAZ-IV	999	825	810